Doctoral Dissertation
博士論文

Study of the sign problem based on the generalized Lefschetz thimble method using gradient flows without blow-up

（ブローアップのないグラディエントフローを用いた一般化レフシェッツシンブル法による符号問題の研究）

A Dissertation Submitted for the Degree of Doctor of Philosophy

December 2020
令和２年１２月博士（理学）申請

Department of Physics, Graduate School of Science,
The University of Tokyo
東京大学大学院理学系研究科物理学専攻

Taichi Ago
吾郷　太一

Abstract

In this dissertation, we study the generalized Lefschetz thimble method using gradient flows without the blow-up, in order to solve the sign problem. The sign problem appears in the numerical simulations of the systems with complex actions. In the systems with complex actions, the integrand of the path integral oscillates and gives an exponentially small expectation value as the volume or the inverse temperature increase. Thus in the numerical simulation, an exponentially huge number of configurations are required. To solve the sign problem, the generalized Lefschetz thimble method is proposed. The idea of the generalized Lefschetz thimble method is complexifying the integration variables and deforming the integration contour owing to Cauchy's integral theorem. In the generalized Lefschetz thimble method, the gradient flow is used to deform the integration contour and suppress the fluctuation of the imaginary part of the action. However, generally the action goes to infinity in a finite time by the gradient flow. The divergence of the action is called the blow-up. The blow-up causes a separation of the integration contour and the ergodicity is broken. To circumvent the blow-up the modification of the gradient flow is proposed. We construct the hybrid Monte Carlo algorithm on the flowed integration contour using the gradient flow without the blow-up. In order to test the validity of the gradient flow without the blow-up, we apply the algorithm to the $(0 + 1)$-dimensional massive Thirring model at finite density, which is a fermionic model with auxiliary fields. Then we show that the sign problem is mild in the algorithm and the result we obtain agrees with the analytic result.

Acknowledgement

First of all, I would like to thank my supervisor, Takeo Moroi for his helpful comment and suggestion with deep insight. Also I would like to thank Yoshio Kikukawa and Hirotsugu Fujii for their fruitful discussion and advice on my work. I am grateful to the members in the theoretical particle physics group for their hospitality and exciting discussion on physics and other topics. Last but not the least, I would like to express my gratitude to my family and friends for their continuous support.

Contents

Chapter 1

Introduction

1.1 Overview

In quantum physics, physical quantities are calculated by the path integral. The path integral can be regarded as the multi-dimensional integral, and the stochastic methods such as the Monte Carlo are used to compute it. The point of this method is that the integrand of the path integral is considered as the Boltzmann weight, and the configurations are generated according to the probability distribution proportional to the weight. Then we obtain the expectation value of an observable effectively by the average over the samples. In quantum field theories, especially, this method is a powerful tool to obtain non-perturbative results, and it has been succeeded to study hadron physics using lattice quantum chromodynamics (QCD). However, when the action is a complex number, we no longer can interpret the integrand as the probability, and the direct Monte Carlo method cannot be applied. This problem is called the sign problem. One may consider the imaginary part of the action as a phase factor and include it in the observable. However, as the volume or the inverse temperature increase, the phase fluctuates rapidly, and the path integral gives an exponentially small phase average. Thus in the numerical simulation, an exponentially huge number of configurations are required, and the sign problem is not resolved. Some of the physically interesting systems have the sign problem. For example, finite-density QCD has a complex action and involves the sign problem. Thus the sign problem is an obstacle of studying neutron matter found in nucleon stars. Moreover, the sign problem appears in real-time dynamics, from which we can obtain the observables such as the viscosity of quark-gluon plasma created in heavy ion collisions. Therefore the development of the approaches solving the sign problem is important.

There have been many approaches which attempt to solve the sign problem. One of the approach is the complex Langevin method [1, 2] based on the stochastic quantization [3], which is referred to as the real Langevin method. In the real Langevin method, the configurations are evolved according to the Langevin equation, which can be regarded

as the Brownian motion. After the thermalization, the configurations are distributed according to the Boltzmann weight. Thus the real Langevin method is the well-established tool to study the quantum many-body systems with a real action. The idea of the complex Langevin method is the complexification of the configuration space. Then we can define the complexified Langevin equation, and consider the evolution of the configurations. However the convergence is not guaranteed as opposed to the real Langevin method. Also even if the convergence is achieved, the expectation value may be incorrect. If the probability distribution of the drift term falls off sufficiently fast, the complex Langevin method is justified [4–6]. For a review of the complex Langevin method, See Ref. [7].

Another approach is deforming the integration path on the complexified configuration space, owing to Cauchy's integral theorem. This approach is the main topic of this dissertation. Using the gradient flow equation, one can define Lefschetz thimbles, on which the imaginary part of the action is constant. In the early attempts, a single thimble was taken into account as the integration contour, under the assumption that it gives the dominant contribution. There are several algorithms to compute the path integral on a single thimble: the Langevin algorithm [8, 9], the Metropolis algorithm [10], and the hybrid Monte Carlo algorithm [11]. Generally the original integration contour is homologically equivalent to the multiple thimbles. To take the contribution of multiple thimbles into account, the generalized thimble method was proposed [12]. In this method, the integration contour is deformed by the gradient flow. However as the flow time increase the contour becomes a disconnected region, and the ergodicity is not satisfied. To avoid this problem, the tempering method [13], and the parallel tempering method [14, 15] are proposed. The idea of these methods is introducing a relaxation parameter, along which the probability distribution is relaxed and the integration contour is merged. Then by the transition along the relaxation parameter, the transition between the configurations which are disconnected is available. In the parallel tempering method, the relaxation parameter is the flow time. For each of the discretized flow times, the configurations are generated simultaneously and exchanged regularly. As an extension of the parallel tempering method, the method where the flow time is also taken into account as the integration region was proposed [16]. There is an attempt to construct an integration contour with some parameters and optimize the parameters so that the sign problem ameliorates. In this approach the integration contour is unrelated to the Lefschetz thimble. To optimize the integration contour, a cost function is defined. Then it is minimized by computing the gradient of it or using the neural network [17–24]. For a review of the Lefschetz thimble method and other path deforming methods, See Ref. [25].

Each of the methods has a strong point and a weak point. The complex Langevin method has the advantage of the cheap computational cost, but it may give incorrect results. On the other hand, the (generalized) Lefschetz thimble method has the disadvantage of the expensive computational cost, since we need to compute the tangent vectors on the deformed integration contour and the determinant of them. However, it has the advantage that mathematically the results are correct as long as the deformed

integration contour is homologically equivalent to the original contour. To apply the Lefschetz thimble method or other path deforming methods to the numerical simulation, we need to specify the deformed integration contour and develop the Monte Carlo algorithm which gives numerically correct results.

The aim of this dissertation is testing the generalized thimble method using the flowed contour by the gradient flow without the blow-up. The flowed contour by the gradient flow without the blow-up is a connected region, and thus the transition between the regions close to different Lefschetz thimbles is possible. We show that in this method the sign problem is mild and the configuration is distributed over the multiple thimbles by applying the method to a toy model.

1.2 Outline of this dissertation

In Chapter 2, a brief review on the Lefschetz thimble method is given. The Lefschetz thimble method was proposed in Refs [8, 9, 11] to solve the sign problem. The sign problem appears in the numerical simulation of the path integral with a complex action. A simple model which has the sign problem is provided to explain the main idea of the Lefschetz thimble method. As one of the numerical implementation, the hybrid Monte Carlo algorithm on the Lefschetz thimble is introduced.

In Chapter 3, the generalized Lefschetz thimble method is reviewed. The generalized Lefschetz thimble method was proposed in Ref [12] to improve a weak point of the Lefschetz thimble method. The original idea of the Lefschetz thimble method does not work in general since many Lefschetz thimbles may contribute to the path integral. In the generalized Lefschetz thimble method the integration contour is deformed to a connected region on which the sign problem is mild. Thus this method may take the contribution of multiple thimbles into account.

In Chapter 4, the idea of the modified gradient flow, which is introduced in order to circumvent the blow-up, is reviewed based on Ref [26]. In the generalized Lefschetz thimble method, the blow-up problem appears as the integration contour is deformed using the conventional gradient flow. The blow-up comes from both the bosonic action and the fermion determinant. It is shown that the improved gradient flow given in this section indeed circumvent the blow-up.

Chapter 5 is the main part of this dissertation, and is based on the author's original work. We construct the algorithm computing the path integral using the gradient flow without the blow-up, based on the hybrid Monte Carlo algorithm on the Lefschetz thimble. Then we apply it to the $(0+1)$-dimensional massive Thirring model at finite density, which is a fermionic model with auxiliary fields. We show the result of the numerical simulation. It shows a good agreement with the analytic result, since the algorithm we construct circumvents the blow-up.

Chapter 2

Lefschetz thimble method

In this chapter, we first provide an intuitive explanation of the sign problem, which appears in the evaluation of the path integrals. Then we explain the Lefschetz thimble method, which may solve the sign problem. We review the basis of the Lefschetz thimble method and algorithms to compute the path integral which has the sign problem.

2.1 Sign problem and Lefschetz thimble method

In quantum field theories, the lattice field theory provides a non-perturbative definition of the path integrals. The Monte Carlo simulation of lattice QCD has been a powerful tool to study hadron physics. However, at low temperature and finite density, the sign problem appears and prevents us from studying the phase diagram from first principles. In this section, we explain the sign problem, which arises from the difficulty of the numerical simulation of the path integral with a complex action. Then, we consider a one-dimensional integral, from which we study a key idea to solve the sign problem.

2.1.1 path integral

In quantum mechanics, the path integral [27, 28] is one of the method to formulate a quantum system and calculate physical quantities. In quantum field theories especially, the partition function in Euclidean formalism is given by

$$Z = \int d\phi(x)\, \exp\left[-S(\phi(x))\right], \tag{2.1}$$

and the expectation value of an observable O is calculated as

$$\langle O \rangle = \frac{1}{Z} \int d\phi(x)\, O(\phi(x)) \exp\left[-S(\phi(x))\right], \tag{2.2}$$

where $S(\phi)$ is the action functional of $\phi(x)$ and x denotes the coordinate point in Euclidean spacetime. Here, we consider the imaginary time or the finite temperature β [1]. For bosonic fields we impose a periodic boundary condition,

$$\phi(x + e^{(i)}L) = \phi(x), \quad i = 1, 2, 3, \tag{2.3}$$

$$\phi(x + e^{(4)}\beta) = \phi(x), \tag{2.4}$$

where $e^{(i)}\,(i = 1, \ldots, 3)$ denote the unit vectors in the direction x_i. For fermionic fields $\psi(x)$, we impose an antiperiodic boundary condition $\psi(x + e^{(4)}\beta) = -\psi(x)$ in the imaginary-time direction. Since the coordinate space $\{x\}$ is continuous, the number of degrees of freedom of the field $\phi(x)$ is infinite and the path integral (2.2) is formally a integral of the infinite-dimensional space. Discretizing the spacetime on the lattice is a way to define the integral rigorously and also enable us to evaluate the integral numerically. After the spacetime is discretized on the lattice, scalar fields and fermionic fields are defined on the lattice points, whereas gauge fields are defined on the links. Then the number of degrees of freedom of the field is finite; it consists of the number of the lattice points (links) and the internal degrees of freedom. For example, gauge fields have vector indices and fermionic fields have spinor indices. Thus, the path integral comes down to the finite-dimensional integral with the large number of integration variables [2]. The continuum limit is considered as the limit in which the lattice volume goes to infinity and the lattice spacing goes to zero.

2.1.2 Monte Carlo method

The Monte Carlo method with importance sampling is mainly used to evaluate multi-dimensional integrals numerically. In this method, the configurations $\phi^{(1)}, \ldots, \phi^{(N)}$ are sampled according to the probability function $P(\phi) \propto \exp(-S(\phi))$. Then, the expectation value of an observable O is estimated by the average of the configurations,

$$\langle O \rangle \approx \frac{1}{N} \sum_{i=1}^{N} O(\phi^{(i)}) + \mathcal{O}(1/\sqrt{N}). \tag{2.5}$$

The statistical error $\mathcal{O}(1/\sqrt{N})$ is independent of the dimension of the integration space, and stochastic approaches such as the Monte Carlo method are powerful to simulate integrals with large numbers of dimensions. The key point of the importance sampling

[1] One may also consider real-time dynamics through the Schwinger-Keldysh formalism [29, 30]. This can be constructed on the lattice. However, simulating the real-time dynamics involves the sign problem. There are studies of Monte Carlo simulations using the complex Langevin method [31, 32] and the Lefschetz-thimble method [33–35].

[2] The measure $d\phi$ is defined properly. In the case of a scalar field, the measure is defined by $d\phi := \prod_{x\in\Gamma} d\phi(x)$, where Γ is the discretized spacetime.

is to find an efficient algorithm generating the configurations $\phi^{(1)}, \ldots, \phi^{(N)}$ according to the probability function $P(\phi)$. In order to generate the configurations, a Markov process is usually used. In this process, a sequence $\phi_{C_0}, \phi_{C_1} \ldots$ of the configurations is produced according to the transition probability $T(\phi_{C_i} \to \phi_{C_{i+1}})$. If the transition probability satisfies the detailed balance condition,

$$\exp(-S(\phi))T(\phi \to \phi') = \exp(-S(\phi'))T(\phi' \to \phi), \tag{2.6}$$

and the stationary distribution exists, the distribution of the configurations ϕ_{C_i} converges to the probability $P(\phi) \propto \exp(-S(\phi))$, as i goes to infinity [3]. To ensure the detailed balance condition, for example Metropolis algorithm and hybrid Monte Carlo algorithm are employed.

2.1.3 Sign problem and reweighting procedure

The method we introduced above works well if the action $S(\phi)$ is real. However, since the probability function needs to be positive, the importance sampling cannot be applied if the action $S(\phi)$ is a complex number or the weight function is oscillatory. This problem is called the sign problem.

One may include the phase factor $\exp(\mathrm{Im}S(\phi))$ in the observable. This is called reweighting procedure. In this procedure, the weight function is replaced by the absolute value of the exponentiation of the action $|\exp(-S)|$, and the integral of this weight function is called the phase-quenched partition function,

$$Z_{\mathrm{PQ}} = \int d\phi \, |\exp\left(-S(\phi)\right)| = \int d\phi \, \exp\left(-\mathrm{Re}S(\phi)\right). \tag{2.7}$$

Then, the expectation value of an observable O with respect to the phase-quenched weight function is given by

$$\langle O \rangle_{\mathrm{PQ}} = \frac{1}{Z_{\mathrm{PQ}}} \int d\phi \, O(\phi) \exp\left[-\mathrm{Re}S(\phi)\right], \tag{2.8}$$

and the expectation value of the observable O with respect to the overall weight function including the phase factor is given by the ratio of the phase-quenched expectation values,

$$\langle O \rangle = \frac{\langle O \exp(-i\mathrm{Im}S(\phi)) \rangle_{\mathrm{PQ}}}{\langle \exp(-i\mathrm{Im}S(\phi)) \rangle_{\mathrm{PQ}}}. \tag{2.9}$$

[3] We abbreviate $T(\phi_{C_i} \to \phi_{C_j})$ as T_{ij} and consider the probability that a configuration ϕ_{C_i} transits to a configuration ϕ_{C_j} after N steps, which is given by $P_{ij}^{(N)} \coloneqq \sum_{i_1,\ldots,i_{N-1}} T_{ii_1} T_{i_1,i_2} \cdots T_{i_{N-1},j}$. If the Markov process satisfies $P_{ij}^{(N)} > 0$ for some N, $P_{ii}^{(N)} \neq 0$ for any N, and $\sum_{n=1}^{\infty} n P_{ii}^{(n)} < \infty$, the stationary distribution $\pi_j \coloneqq \lim_{N\to\infty} P_{ij}^{(N)}$ exists.

If the phase fluctuation is mild and the cancellation between the contributions from the positive and negative signs does not occur frequently, both the numerator and the denominator on the right-hand side of Eq. (2.9) are finite so that we can numerically evaluate the ratio with sufficient accuracy. However, conversely if the phase cancellation occurs frequently, a huge number of configurations are required so that the statistical error is much smaller than the mean of the phase average, $|\langle \exp(-i\mathrm{Im}S(\phi))\rangle_{\mathrm{PQ}}| \gg 1/\sqrt{N}$. In the physical systems the phase average vanishes exponentially as we increase the volume V or the inverse temperature β:

$$\langle \exp(-i\mathrm{Im}S(\phi))\rangle_{\mathrm{PQ}} = \frac{\int d\phi \, \exp\left(-S(\phi)\right)}{\int d\phi \, \exp\left(-\mathrm{Re}S(\phi)\right)} \approx \frac{\exp(-\beta V f)}{\exp(-\beta V f_{\mathrm{PQ}})} = e^{-\beta V (f - f_{\mathrm{PQ}})}, \quad (2.10)$$

where f and f_{PQ} denote the free energy density in the original and phase-quenched systems. We note that $f - f_{\mathrm{PQ}} > 0$, since the numerator on right-hand side of the first equation in Eq. (2.10) has a phase factor $\exp\left(-i\mathrm{Im}S(\phi)\right)$ in the integrand. Thus, the computational cost to achieve the sufficiently small statistical error in evaluating $\langle O \rangle$ grows exponentially as we increase the volume or decrease the temperature:

$$N \gg e^{2\beta V (f - f_{\mathrm{PQ}})}. \quad (2.11)$$

This means the reweighting procedure does not work practically, and the sign problem again appears. Moreover the situation is worse when the action is pure imaginary, since reweighting procedure cannot be applied. Thus the simulation of the real-time dynamics suffers from the severe sign problem.

2.1.4 Example of complexified contour: Airy integral

Although the numerical simulations of the integrals with the complex actions are quite difficult in a direct way, there are cases where the sign problem disappears by using the alternative description based on the complex analysis. To explain how to circumvent it, now we consider the following one-dimensional integral:

$$Z(t) = \int_{-\infty}^{\infty} \frac{d\phi}{2\pi} \exp(-S(\phi, t)), \quad S(\phi, t) = -i(\phi^3/3 + t\phi). \quad (2.12)$$

$Z(t)$ is known as Airy integral. Since the action is a pure imaginary number, the convergence of the integral as ϕ goes to infinity is slow. However, owing to Cauchy's integral theorem, after the analytic continuation of the integration variable we can deform the integration contour keeping the integral unchanged, and make the integrand have a good convergence property along the contour. We can find the steepest descent and ascent paths for each of the critical points $\phi_{\mathrm{crit.}}$, which satisfy $\partial S/\partial\phi(\phi_{\mathrm{crit.}}, t) = 0$. The critical

point is called the saddle point especially in one-dimensional integral because of this property. Along the steepest descent and ascent paths, the tangent vector $e^{i\theta}$ is determined so that

$$S(\phi + \varepsilon e^{i\theta}, t) \approx S(\phi, t) + \varepsilon e^{i\varphi_S} \left|\frac{\partial S}{\partial \phi}\right| e^{i\theta}, \quad \frac{\partial S}{\partial \phi} = e^{i\varphi_S} \left|\frac{\partial S}{\partial \phi}\right| \tag{2.13}$$

is maximized and minimized in the real part, respectively. It indicates $\theta = -\varphi_S$ and $\theta = \pi - \varphi_S$, and the imaginary part of the action $\mathrm{Im}S$ is constant along them. Thus the steepest descent path satisfies the properties required for the numerical simulation, that is, the fast convergence and the constant phase factor. Let us consider Airy integral with $t > 0$. After complexifing the integration variable $\phi \in \mathbb{C}$, the critical points are given by the equation,

$$\frac{\partial S}{\partial \phi}(\phi_{\text{crit.}}, t) = -i(\phi_{\text{crit.}}^2 + t) = 0 \Leftrightarrow \phi_{\text{crit.}} = \pm i\sqrt{t}. \tag{2.14}$$

There are two critical points and we need to choose the relevant steepest descent path. The integrand is convergent only if $\mathrm{Re}(\phi^3) > 0$ as $|\phi|$ goes to infinity, and we denote the corresponding regions of $2\pi/3 < \arg(\phi) < \pi$, $0 < \arg(\phi) < \pi/3$ and $4\pi/3 < \arg(\phi) < 5\pi/3$ as the regions A, B and C as shown in Fig. 2.1(Left). The starting and ending points at infinity of the deforming contour need to be in these regions. Therefore, we can deform the integration contour to the steepest descent path with the critical point $\phi_{\text{crit.}} = +i\sqrt{t}$ as shown in Fig. 2.1(Left). As shown in Fig. 2.1(Right), although the integrand of the original contour is oscillatory (solid red line), that of the deformed contour damps out (dashed blue line).

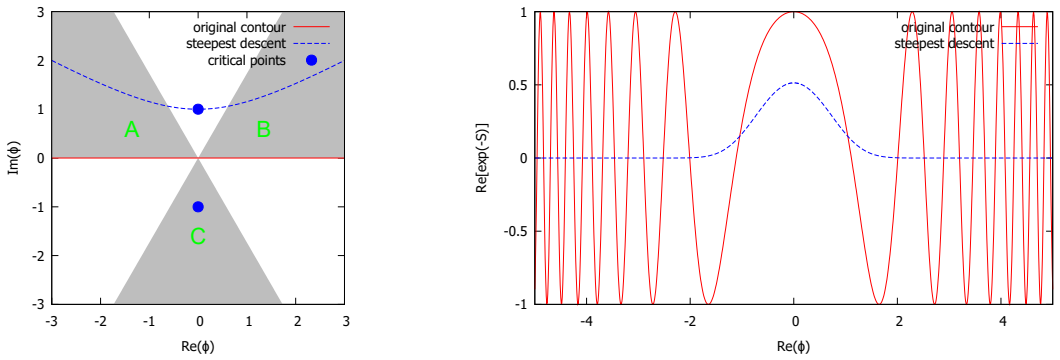

Figure 2.1: Two integration contours for Airy integral ($t = 1$). (Left) Deformation of the integration contour on the complex ϕ-plane. In the gray regions the integrand is asymptotically convergent. (Right) Behavior of the integrands $\mathrm{Re}(\exp(-S))$ for the original contour and the deformed contour.

Let us consider a generic case where t is a complex number. Along the real axis the integrand is divergent, but we can define the contour where the starting and ending points at infinity go to the regions A and B so that the integral is convergent. We denote the

steepest descent and ascent paths associated with the critical point $\phi_{\text{crit.}}$ as $\mathcal{J}_{\phi_{\text{crit.}}}$ and $\mathcal{K}_{\phi_{\text{crit.}}}$. If the phase of the parameter t is small enough, then we can deform the original contour to the steepest descent path associated with the critical point $i\sqrt{t}$ as is the case for $t > 0$:

$$Z(t) = \int_{-\infty}^{\infty} \frac{d\phi}{2\pi} \exp(-S(\phi, t)) = \int_{\mathcal{J}_{i\sqrt{t}}} \frac{d\phi}{2\pi} \exp(-S(\phi, t)). \tag{2.15}$$

We note that the steepest descent path associated with the critical point $-i\sqrt{t}$ does not contribute to the integral (2.15), but the topological structure of the steepest descent paths changes drastically at $\arg(t) = 0$, which is called the Stokes jump. As shown in Fig. 2.2, the steepest descent path $\mathcal{J}_{-i\sqrt{t}}$ connects with the regions of C and A for $\arg(t) < 0$ but C and B for $\arg(t) > 0$. The Stokes phenomenon may happen when the multiple critical points share the same value of the imaginary part of the action $\text{Im}S$, and both the steepest descent and ascent paths connect these critical points. The Stokes jumps suggest the possibility of the drastic change of the steepest descent path contributing to the integral. If we define the original integration contour as the one that connects with the regions of C and A or C and B, then the contributing contours change at $\arg(t) = 0$.

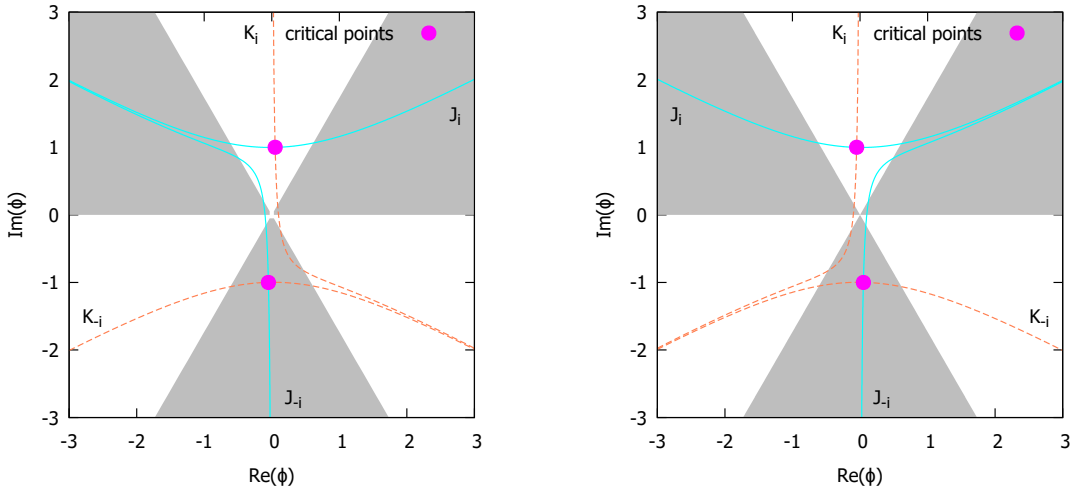

Figure 2.2: Stokes jump at $\arg(t) = 0$ in the complex ϕ-plane. (Left) $t = \exp(-\delta i)$. (Right) $t = \exp(+\delta i)$. Here we put $\delta = 0.1$ in both cases.

Since the action S has two critical points $\phi_{\text{crit.}} = \pm i\sqrt{t}$, the candidates for the parameter t of the Stokes jumps are given by the condition,

$$\text{Im}S(i\sqrt{t}, t) = \text{Im}S(-i\sqrt{t}, t) \Leftrightarrow t = 0, e^{\pm 2\pi i/3}. \tag{2.16}$$

As shown in Fig. 2.3 for $t = e^{2\pi i/3}$, the Stokes jump occurs at $t = e^{\pm 2\pi i/3}$. We note that when $2\pi/3 < \arg(t) < 4\pi/3$, both of the steepest descent path associated with the critical

points $\phi_{\text{crit.}} = \pm i\sqrt{t}$ contribute to the integral; that is, they are topologically equivalent to the original integration contour:

$$Z(t) = \int_{\mathcal{J}_{-i\sqrt{t}}} \frac{d\phi}{2\pi} \exp(-S(\phi, t)) + \int_{\mathcal{J}_{+i\sqrt{t}}} \frac{d\phi}{2\pi} \exp(-S(\phi, t)). \tag{2.17}$$

Thus in general, it is an important task to determine which steepest descent paths contribute to the integral when we use the steepest descent method.

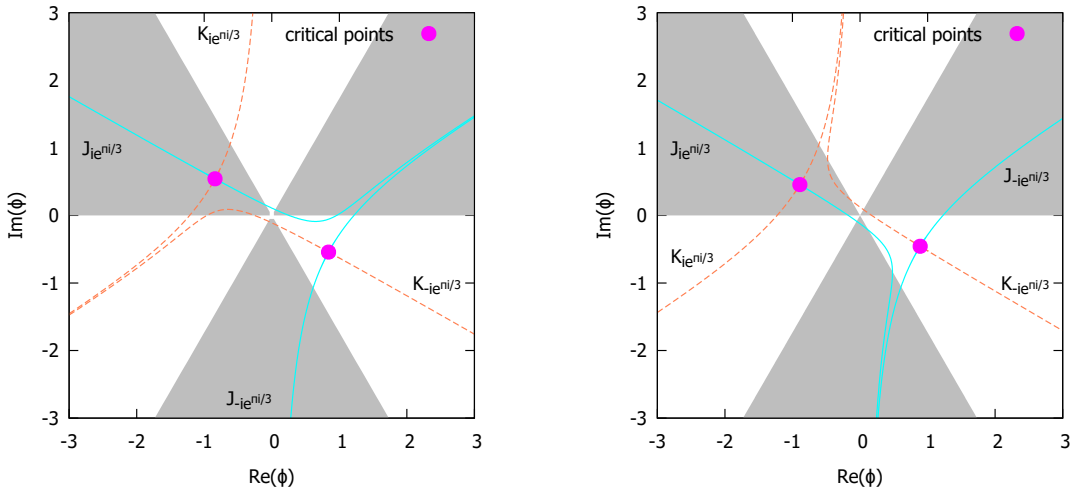

Figure 2.3: Stokes jump at $\arg(t) = 2\pi/3$ in the complex ϕ-plane. (Left) $t = \exp(2\pi i/3 - \delta i)$. (Right) $t = \exp(2\pi i/3 + \delta i)$. Here we put $\delta = 0.1$ in both cases.

2.2 Complexification in multiple dimensions

In this section, we generalize the steepest descent method in multi-dimensional theory. In multi-dimensional theory, Lefschetz thimbles correspond to steepest descent paths. Lefschetz thimbles are constructed using the gradient flow, along which the imaginary part of the action is constant.

2.2.1 Generalized Cauchy's integral theorem

First, let us consider the theory with n real degrees of freedom $x = (x_1, \ldots, x_n)$. We assume that x takes the value on $\mathcal{C}_{\mathbb{R}}$ ($\subseteq \mathbb{R}^n$). The partition function of this theory is given by

$$Z = \int_{\mathcal{C}_{\mathbb{R}}} d^n x \, \exp(-S(x)), \tag{2.18}$$

and our main purpose is to evaluate the expectation value of an observable $O(x)$,

$$\langle O \rangle = \frac{1}{Z} \int_{\mathcal{C}_{\mathbb{R}}} d^n x \, O(x) \exp(-S(x)). \tag{2.19}$$

We complexify the real variable as $x \in \mathcal{C}_{\mathbb{R}} \to z \in \mathbb{C}^n$ and assume that $S(z)$ is a holomorphic function in $\mathbb{C}^n \to \mathbb{C}$. Due to Cauchy's integral theorem in multiple dimensions, we may deform the contour $\mathcal{C}_{\mathbb{R}}$ to the contour $\mathcal{C}$ in the complex space $\mathbb{C}^n$:

$$Z = \int_{\mathcal{C}} d^n z \, \exp(-S(z)). \tag{2.20}$$

Eq. (2.20) is formally an integral over the n complex variables, and one may take the definition as follows:

$$\int_{\mathcal{C}} f(z) dz_1 \cdots dz_n = \int_{\mathbb{M}} f(\varphi(\xi)) \det J(\xi) d\xi_1 \cdots d\xi_n, \tag{2.21}$$

where φ maps n-dimensional real manifold $\mathbb{M}$ by the real coordinates $\xi = (\xi_1, \ldots, \xi_n)$ to the contour $\mathcal{C}$ in the n-dimensional complex space, as $z_i = \varphi_i(\xi_1, \ldots, \xi_n)$. $\det J(x)$ is the determinant of the Jacobian matrix,

$$J_{ij}(\xi) = \frac{\partial z_i}{\partial \xi_j}, \tag{2.22}$$

and $\det J(\xi)$ is a complex number in general. Here, we assume $\mathcal{C}$ and thus $\mathbb{M}$ have no boundary. We note that the integrand of the right-hand side in Eq. (2.21) is complex, but we may take the right-hand side in Eq. (2.21) as the sum of the real part and the imaginary part, which are the integrals of the real function. Now we consider two such integration contours $\mathcal{C}_0$ and $\mathcal{C}_1$ that we can deform smoothly to each other. We can define a continuous map $\Phi(\xi, t) : \mathbb{M} \times [0, 1] \to \mathbb{C}^n$ such that $\Phi(\xi, 0)$ maps ξ onto $\mathcal{C}_0$ and $\Phi(\xi, 1)$ maps ξ onto $\mathcal{C}_1$. Then we have

$$\int_{\mathcal{C}_1 - \mathcal{C}_0} f(z) dz_1 \cdots dz_n = \int_{\mathbb{M} \times [0,1]} \frac{\partial}{\partial t} \left[f(\Phi(\xi, t)) \det J(\xi) \right] dt d\xi_1 \cdots d\xi_n. \tag{2.23}$$

We note that the following identity holds:

$$\frac{\partial}{\partial t} \left[f(\Phi(\xi, t)) \det J(\xi) \right] = \sum_{i=1}^{n} \frac{\partial}{\partial \xi_i} \left[f(\Phi(\xi, t)) \det J(\xi)|_{\xi_i \to t} \right], \tag{2.24}$$

where

$$J(\xi)_{kl}|_{\xi_i \to t} = \begin{cases} \dfrac{\partial z_k}{\partial \xi_l} & (l \neq i), \\ \dfrac{\partial z_k}{\partial t} & (l = i). \end{cases} \tag{2.25}$$

Therefore the right-had side of Eq. (2.23) vanishes, and we obtain the generalized Cauchy's integral theorem,

$$\int_{\mathcal{C}_0} f(z) dz_1 \cdots dz_n = \int_{\mathcal{C}_1} f(z) dz_1 \cdots dz_n. \tag{2.26}$$

2.2.2 Gradient flow and Lefschetz thimble

Now, we are interested in deforming the contour where the sign problem vanishes. Picard-Lefschetz theory, which is the analogue of Morse theory for the complex space, is applied to find such a contour [36, 37] [4]. To perform the deformation, the gradient flow is introduced through the differential equation,

$$\frac{d}{dt}z_i(t) = \left(\frac{\partial S}{\partial z_i}\right)^*, \tag{2.27}$$

where the complex conjugate of $z = a + ib\,(a, b \in \mathbb{R})$ is denoted as $z^* = a - ib$. Here the flow time t is introduced, and initial point $z_i(0)$ is mapped to $z_i(t)$ according to the gradient flow equation (2.27). Since critical points z_σ satisfy $\partial S/\partial z_i(z_\sigma) = 0$, they are the fixed points of the gradient flow. Associated with a critical point z_σ, we can define two types of submanifolds in $\mathbb{C}^n$:

$$\mathcal{J}_\sigma \coloneqq \{z(0) \in \mathbb{C} \mid z(-\infty) = z_\sigma\}, \tag{2.28}$$

$$\mathcal{K}_\sigma \coloneqq \{z(0) \in \mathbb{C} \mid z(+\infty) = z_\sigma\}. \tag{2.29}$$

The former corresponds to the steepest descent path for the one-dimensional theory and the latter corresponds to the steepest ascent path for the one-dimensional theory. We call the submanifold $\mathcal{J}_\sigma$ the Lefschetz thimble and the submanifold $\mathcal{K}_\sigma$ the dual thimble.

Using Eq. (2.27) we have

$$\frac{d}{dt}\mathrm{Re}S = \frac{1}{2}\left(\frac{\partial S}{\partial z_i}\frac{dz_i}{dt} + \left(\frac{\partial S}{\partial z_i}\right)^*\left(\frac{dz_i}{dt}\right)^*\right) = \left(\frac{\partial S}{\partial z_i}\right)^*\frac{\partial S}{\partial z_i} \geq 0, \tag{2.30}$$

$$\frac{d}{dt}\mathrm{Im}S = \frac{1}{2i}\left(\frac{\partial S}{\partial z_i}\frac{dz_i}{dt} - \left(\frac{\partial S}{\partial z_i}\right)^*\left(\frac{dz_i}{dt}\right)^*\right) = 0. \tag{2.31}$$

We note that $\exp(-\mathrm{Re}S)$ monotonically decreases (increases) as the point z on $\mathcal{J}_\sigma$ ($\mathcal{K}_\sigma$) flows away from the critical point, and the phase factor $\exp(-\mathrm{Im}S)$ is constant along both $\mathcal{J}_\sigma$ and $\mathcal{K}_\sigma$. If a critical point z_σ is isolated, the Hessian matrix of $-\mathrm{Re}S$ with respect to the $2n$ real degrees of freedom $\mathrm{Re}(z_k), \mathrm{Im}(z_k)\,(k = 1, \ldots, n)$ has n positive eigenvalues and n negative eigenvalues. Thus both $\mathcal{J}_\sigma$ and $\mathcal{K}_\sigma$ are the n-dimensional submanifolds. Since $-\mathrm{Re}S(z) \leq -\mathrm{Re}S(z_\sigma)$ for $z \in \mathcal{J}_\sigma$ and $-\mathrm{Re}S(z_\sigma) \leq -\mathrm{Re}S(z)$ for $z \in \mathcal{K}_\sigma$, $\mathcal{J}_\sigma$ and $\mathcal{K}_\sigma$ has a intersection only at the critical point z_σ. On the other hand, when the Stokes phenomenon does not occur and thus the critical points are not connected by the gradient

[4] $-\mathrm{Re}S(z)$ correspond to the Morse function h in Morse theory. The Morse function is a function such that the Hessian matrix is invertible at the critical points. The number of negative eigenvalues of this matrix is called the Morse index. The Morse function is a powerful tool to analyze the relative homology group. It gives Morse inequalities, which state that the rank of the n th homology group is less than or equal to the number of critical points with the Morse index n. If the equalities hold especially, h is called a perfect Morse function.

flow, $\mathcal{J}_{\sigma_1}$ and $\mathcal{K}_{\sigma_2}$ with different critical points $z_{\sigma_1} \neq z_{\sigma_2}$ do not intersect with each other. We denote the intersection of $\mathcal{J}_{\sigma_1}$ and $\mathcal{K}_{\sigma_2}$ as [5)]

$$\langle \mathcal{J}_{\sigma_1}, \mathcal{K}_{\sigma_2} \rangle = \delta_{\sigma_1 \sigma_2}. \tag{2.32}$$

According to Picard-Lefschetz theory, the contour $\mathcal{C}_{\mathbb{R}}$ over which the integral converges is homologically equivalent to a linear combination of the Lefschetz thimbles $\mathcal{J}_\sigma$:

$$\mathcal{C}_{\mathbb{R}} \simeq \sum_{\sigma \in \Sigma} n_\sigma \mathcal{J}_\sigma, \quad n_\sigma \in \mathbb{Z}, \tag{2.33}$$

where Σ denotes the set of the critical points, and from Eq. (2.32) the coefficient n_σ is given by [6)]

$$n_\sigma = \langle \mathcal{C}_{\mathbb{R}}, \mathcal{K}_\sigma \rangle. \tag{2.34}$$

Since the integration contour $\mathcal{C}_{\mathbb{R}}$ can be deformed to the combination of the Lefschetz thimbles according to Eq. (2.33), the partition function is given by

$$Z = \sum_{\sigma \in \Sigma} n_\sigma \exp(-S(z_\sigma)) Z_\sigma, \tag{2.35}$$

where

$$Z_\sigma = \int_{\mathcal{J}_\sigma} d^n z \, \exp\left[-\mathrm{Re}(S(z) - S(z_\sigma))\right]. \tag{2.36}$$

Therefore, if an observable $O(x)$ is holomorphic in $\mathbb{C}^n \to \mathbb{C}$, the expectation value of $O(x)$ is now given by

$$\langle O \rangle = \frac{1}{Z} \sum_{\sigma \in \Sigma} n_\sigma \exp(-S(z_\sigma)) Z_\sigma \langle O \rangle_{\mathcal{J}_\sigma}, \tag{2.37}$$

where

$$\langle O \rangle_{\mathcal{J}_\sigma} = \frac{1}{Z_\sigma} \int_{\mathcal{J}_\sigma} d^n z \, \exp\left[-\mathrm{Re}(S(z) - S(z_\sigma))\right] O(z). \tag{2.38}$$

We note that the set of critical points Σ is divided into the three subsets:

$$\Sigma_0 \coloneqq \left\{ \sigma \in \Sigma \mid z_\sigma \in \mathcal{C}_{\mathbb{R}} \right\}, \tag{2.39}$$

$$\Sigma_{\geq} \coloneqq \left\{ \sigma \in \Sigma \;\middle|\; z_\sigma \notin \mathcal{C}_{\mathbb{R}}, -\mathrm{Re}S(z_\sigma) \geq \max_{x \in \mathcal{C}_{\mathbb{R}}} \left[-\mathrm{Re}S(x)\right] \right\}, \tag{2.40}$$

$$\Sigma_{<} \coloneqq \left\{ \sigma \in \Sigma \;\middle|\; z_\sigma \notin \mathcal{C}_{\mathbb{R}}, -\mathrm{Re}S(z_\sigma) < \max_{x \in \mathcal{C}_{\mathbb{R}}} \left[-\mathrm{Re}S(x)\right] \right\}. \tag{2.41}$$

[5)] The sign of the intersection number depends on the orientations of $\mathcal{J}_\sigma$ and $\mathcal{K}_\sigma$. For example, we can introduce the real local coordinates $\xi_1, \ldots, \xi_n$ for $\mathcal{J}_\sigma$ and $\eta_1, \ldots, \eta_n$ for $\mathcal{K}_\sigma$ at the vicinity of the intersecting point. Then, we can give a positive intersection number if the determinant of the Jacobian matrix $\partial(\mathrm{Re}(z_1), \ldots, \Re(z_n), \mathrm{Im}(z_1), \ldots, \mathrm{Im}(z_n))/\partial(\xi_1, \ldots, \xi_n, \eta_1, \ldots, \eta_n)$ is positive and vice versa. Here, we introduce appropriate orientations of $\mathcal{J}_\sigma$ and $\mathcal{K}_\sigma$ so that they have a positive intersection number.

[6)] The contour $\mathcal{C}_{\mathbb{R}}$ may intersect with $\mathcal{K}_\sigma$ more than once. In that case, n_σ is given by $n_+ - n_-$, where n_+ (n_-) is the number of the intersections with positive (negative) signs.

$\mathcal{K}_\sigma$ associated with the critical point belonging to $\Sigma_\geq$ do not intersect with the original integration contour $\mathcal{C}_\mathbb{R}$, since $-\mathrm{Re}S(z) > -\mathrm{Re}S(z_\sigma)$ for $z \in \mathcal{K}_\sigma - \{z_\sigma\}$, whereas $-\mathrm{Re}S(z) \leq -\mathrm{Re}S(z_\sigma)$ for $z \in \mathcal{C}_\mathbb{R}$. Thus the associated Lefschetz thimbles $\mathcal{J}_\sigma$ do not contribute to the path integral. The Lefschetz thimbles $\mathcal{J}_\sigma$ associated with the critical point belonging to $\Sigma_<$ may or may not contribute to the integral (2.35), but the contribution is exponentially suppressed by the relative weight $\exp(-S(z_\sigma))$. The critical points belonging to Σ_0 satisfy $\langle \mathcal{C}_\mathbb{R}, \mathcal{K}_\sigma \rangle = \pm 1$ since $\mathcal{K}_\sigma$ intersects with $\mathcal{C}_\mathbb{R}$ at the critical point. In particular, with respect to the classical vacuum $z_{\text{vac.}}$, which is a critical point on the original contour $\mathcal{C}_\mathbb{R}$ and satisfies

$$-\mathrm{Re}S(z_{\text{vac.}}) = \max_{x \in \mathcal{C}_\mathbb{R}} \left[-\mathrm{Re}S(x)\right], \tag{2.42}$$

the associated Lefschetz thimbles $\mathcal{J}_{\text{vac.}}$ contribute to the integral with the largest relative weight $\exp(-S(z_\sigma))$ among all the thimbles contributing to the integral. Therefore, if the model has a classical vacuum $z_{\text{vac.}}$, we may approximate the expectation value of an observable $O(x)$ by the Lefschetz thimble associated with the classical vacuum:

$$\langle O \rangle \approx \langle O \rangle_{\mathcal{J}_{\text{vac.}}}. \tag{2.43}$$

2.2.3 Tangent Vectors

We can parametrize the point z on the thimble $\mathcal{J}_\sigma$ by the initial point $z(0)$ in the vicinity of the critical point and the flow time t when the initial point $z(0)$ arrives at the point $z = z(t)$. In the vicinity of the critical point z_σ, the gradient flow equation (2.27) can be linearized as

$$\frac{d}{dt}(z_i(t) - z_\sigma) = H^*_{ij}(z^*_j(t) - z^*_{\sigma j}), \quad H_{ij} \coloneqq \frac{\partial^2 S}{\partial z_i \partial z_j}(z_\sigma). \tag{2.44}$$

According to the Takagi factorization theorem [38], the complex symmetric matrix H can be factorized into $U^T \mathrm{diag}(\lambda^1, \ldots, \lambda^n) U$, where U is a unitary matrix and λ^α are non-negative numbers. In other words, using orthonormal complex vectors v^α_i, we have

$$H_{ij} v^\alpha_j = \lambda^a v^{\alpha *}_i. \tag{2.45}$$

We note that the set of complex vectors $\{v^\alpha_j\}$ and $\{iv^\alpha_j\}$ spans $\mathbb{C}^n$ with real coefficients. Eq. (2.44) is a linear differential equation; that is, if $u^1(t), u^2(t) \in \mathbb{C}^n$ are the solution of $z_i - z_\sigma$ in Eq. (2.44), $c^1 u(t)^1 + c^2 u^2(t)$, $(c^1, c^2 \in \mathbb{R})$ is also the solution. Thus we may substitute for $z_i(t) - z_\sigma$ the linear combination of complex vectors $\{v^\alpha_j\}$ and $\{iv^\alpha_j\}$ with real coefficients, and the solution of Eq. (2.44) can be written as

$$z_j(t) - z_{\sigma j} = \sum_{\alpha=1}^{n} \xi^\alpha v^\alpha_j e^{\lambda^\alpha t} + \sum_{\alpha=1}^{n} \eta^\alpha i v^\alpha_j e^{-\lambda^\alpha t}, \quad \xi^\alpha, \eta^\alpha \in \mathbb{R}\,(\alpha = 1, \ldots, n). \tag{2.46}$$

Now we assume the critical point is isolated [7]. Then the first term in the right-hand side of Eq. (2.46) converges to zero as $t \to -\infty$, whereas the second term converges to zero as $t \to -\infty$. From the definition of $\mathcal{J}_\sigma$ and $\mathcal{K}_\sigma$, v_j^α and iv_j^α are the tangent vectors of $\mathcal{J}_\sigma$ and $\mathcal{K}_\sigma$ at the critical point, respectively. Thus in the vicinity of the critical point, the point z on the Lefschetz thimble is parametrized by the real variables ξ^α as $z_j \approx z_{\sigma j} + \xi^\alpha v_j^\alpha$. The tangent vectors V_i^α at a generic point are obtained by solving the differential equation,

$$\frac{d}{dt}V_i^\alpha(t) = \left(\frac{\partial^2 S}{\partial z_i \partial z_j}\right)^* V_j^{\alpha *}(t), \tag{2.47}$$

which is the consequence of the infinitesimal variation δz in Eq. (2.27). The basis of tangent vectors $\{V_i^\alpha\}$ is not orthonormal in general, but we can derive the coefficients ξ^α, η^α of the vector $\xi^\alpha V_j^\alpha + \eta^\alpha i V_j^\alpha \in \mathbb{C}^n$ by using the reality condition,

$$V_i^{\alpha *} V_i^\beta - V_i^{\beta *} V_i^\alpha = 0, \tag{2.48}$$

which holds since from Eq. (2.27) we have

$$\frac{d}{dt}(V_i^{\alpha *} V_i^\beta - V_i^{\beta *} V_i^\alpha) = 0, \tag{2.49}$$

and the initial vectors at the critical point are orthonormal. We can define an inner product of two complex vectors $u, v \in \mathbb{C}^n$ as

$$\langle u, v \rangle := \mathrm{Re}(u_j^* v_j) = \mathrm{Re}(u_j)\mathrm{Re}(v_j) + \mathrm{Im}(u_j)\mathrm{Im}(v_j). \tag{2.50}$$

Then the reality condition (2.48) can be expressed as $\langle V^\alpha, iV^\beta \rangle = 0$.

2.2.4 Parametrization

We can parametrize any point z on the thimble $\mathcal{J}_\sigma$ by (e, t) through solving Eq. (2.27) up to the flow time t with the initial condition $z(0) = z_\sigma + \varepsilon e$, where e is the unit vector on the tangent space, and ε is a sufficiently small constant so that the linear approximation is valid. We can also compute the associated tangent vector through solving Eq. (2.47) with the initial condition $V_i^\alpha(0) = v_i^\alpha$.

[7] For example, in the complex scalar field theory with the finite chemical potential, the global minimum is degenerate if the U(1) symmetry is spontaneously broken. In that case, We can resolve the degeneracy by introducing a term which explicitly breaks the symmetry: $\varepsilon \sum_{a,x} \phi_a(x)$, where $\phi_a(x)$ $(a = 1, 2)$ denotes the real field variables of the complex scalar field $\phi(x) = \phi_1(x) + i\phi_2(x)$ on the lattice [8, 9]. These real variables are complexified to deform the integration contour. Then the physical result is obtained by extrapolating to $\varepsilon \to 0$.

2.3 Summary of the algorithm

In this section, we review the hybrid Monte Carlo approaches on the Lefschetz thimble, which was proposed in Refs. [11]. As discussed in the previous section, we assume a single Lefschetz thimble contributes to the path integral. Then we can use the Markov chain Monte Carlo method where the new configurations are generated according to the probability distributed around the old configurations on the connected space. The hybrid Monte Carlo method is the method often used in the lattice simulations since the configurations are generated with the high acceptance rate, compared to the Gaussian random walk proposal in the Metropolis method [39].

2.3.1 Hybrid Monte Carlo

On the real space $\mathbb{R}^n$, the hybrid Monte Carlo update is given by the following procedure:

1. Set the initial configuration $\phi \in \mathbb{R}^n$.
2. Generate π according to the Gaussian distribution $P_G(\pi) \propto e^{-\pi^2/2}$.
3. Propose a configuration (ϕ', π') by a reversible map, where the transition probability satisfies the equality, [8)]
$$P_H((\phi, \pi) \to (\phi', \pi')) = P_H((\phi', -\pi') \to (\phi, -\pi)). \tag{2.51}$$
4. Accept the proposed configuration (ϕ', π') by the probability,
$$P_A((\phi, \pi) \to (\phi', \pi')) = \min\{1, e^{-\Delta H}\}, \tag{2.52}$$
where ΔH is the variation of the Hamiltonian
$$H = \frac{1}{2}\pi^2 + S(\phi). \tag{2.53}$$

By repeating the update, we obtain the sequence of the configurations $\phi^{(1)}, \ldots, \phi^{(n_{\rm traj})}$.

This update satisfies the detailed balance condition as follows. The transition probability restricted to the variables ϕ is given by

$$P_M(\phi \to \phi') = \int d\pi d\pi' \, P_G(\pi) P_H((\phi, \pi) \to (\phi', \pi')) P_A((\phi', \pi') \to (\phi, \pi)). \tag{2.54}$$

From the identity,

$$e^{-H(\phi,\pi)} P_A((\phi, \pi) \to (\phi', \pi')) = e^{-H(\phi',\pi')} P_A((\phi', \pi') \to (\phi, \pi)), \tag{2.55}$$

[8)] The probability function P_H is a delta function if the map $(\phi, \pi) \to (\phi', \pi')$ is deterministic.

and the reversibility (2.55), we have

$$e^{-S(\phi)}P_M(\phi \to \phi') = e^{-S(\phi')}P_M(\phi' \to \phi). \tag{2.56}$$

The update efficiently generates the configurations according to the probability $P(\phi) \propto e^{-S(\phi)}$, if the variation of the Hamiltonian ΔH is small and the updated configurations are distant. Now we consider the molecular dynamics to find a map $(\phi, \pi) \to (\phi', \pi')$ which preserves the Hamiltonian. The molecular dynamics evolution is considered by

$$\frac{d\phi}{d\tau}(\tau) = \frac{\delta H}{\delta \pi} = \pi(\tau), \tag{2.57}$$

$$\frac{d\pi}{d\tau}(\tau) = \frac{\delta H}{\delta \phi} = -\frac{\partial S}{\partial \phi}(\phi(\tau)). \tag{2.58}$$

Here a Monte Carlo time τ is introduced. In analogy to classical mechanics, the Hamiltonian is invariant. We stress that Eqs. (2.57) and (2.58) are not the equations of motion of the underlying theory, but those associated to the artificial Hamiltonian H. If the variable τ is continuous and we solve the dynamics up to the time τ_f, the proposed configuration $(\phi(\tau_f), \pi(\tau_f))$ in the hybrid Monte Carlo update is alway accepted. However, in the numerical simulation the variable τ need to be discretized by the number of steps $n_{\rm step}$. The discretization is simply implemented by the leap-frog:

$$\pi(n+1/2) = \pi(n) - \frac{1}{2}\Delta\tau \frac{\partial S}{\partial \phi}(n), \tag{2.59}$$

$$\phi(n+1) = \pi(n) + \Delta\tau\pi(n+1/2), \tag{2.60}$$

$$\pi(n+1) = \pi(n+1/2) - \frac{1}{2}\Delta\tau \frac{\partial S}{\partial \phi}(n+1), \tag{2.61}$$

where $\Delta\tau$ is the step size and given by $\tau_f/n_{\rm step}$. We note that the leap-flog is reversible $(\phi(n+1), -\pi(n+1)) \to (\phi(n), -\pi(n))$ and the violation of the Hamiltonian is $\mathcal{O}(\Delta\tau^2)$ due to the reversibility.

2.3.2 Molecular dynamics with constrains

Now, we are interested in formulating the hybrid Monte Carlo on the thimble $\mathcal{J}_\sigma$. Since the thimble $\mathcal{J}_\sigma$ is a curved space, we need to introduce the molecular dynamics with constraints by the equation of motion,

$$\frac{dz_i}{d\tau} = w_i, \tag{2.62}$$

$$\frac{dw_i}{d\tau} = -\left(\frac{\partial S}{\partial z_i}\right)^* - iV_i^\alpha \lambda^\alpha, \tag{2.63}$$

where $\lambda^\alpha \in \mathbb{R}\,(\alpha = 1, \ldots, n)$ are the Lagrange multipliers. Here we introduced the complex-valued momenta w_i. Since z_i are constrained on the thimble and Eq. (2.62) holds, w_i are constrained on the tangent space $T_z\mathcal{J}_\sigma$. These constraints are represented as

$$z = \Phi(e, t), \quad \langle w, iV^\alpha \rangle = 0. \tag{2.64}$$

Φ is the map given by the flow (2.27) up to the flow time t of the initial point $z(0) = z_\sigma + \varepsilon e$, where $e \in T_{z_\sigma}\mathcal{J}_\sigma$ and $\|e\| = 1$. The gradient flow equation (2.27) is solved numerically by the Runge-Kutta method. The Hamiltonian is given by

$$H = \frac{1}{2} w_i^* w_i + \mathrm{Re}[S(z)], \tag{2.65}$$

and it is conserved since

$$\begin{aligned} \frac{dH}{d\tau} &= \frac{1}{2}\left(\frac{dw_i}{d\tau}^* w_i + w_i^* \frac{w_i}{d\tau}\right) + \mathrm{Re}\left(\frac{\partial S}{\partial z_i}\frac{dz_i}{d\tau}\right) \\ &= -\langle w, iV^\alpha \rangle \lambda^\alpha \\ &= 0. \end{aligned} \tag{2.66}$$

To implement the molecular dynamics in the numerical simulation, we may discretize the time τ as follows:

$$w_i(n+1/2) = w_i(n) - 1/2\Delta\tau \left(\frac{\partial S}{\partial z_i}\right)^*\Big|_{z(n)} - 1/2\Delta\tau i V_i^\alpha(z(n))\lambda_1^\alpha, \tag{2.67}$$

$$z_i(n+1) = z_i(n) + \Delta\tau w_i(n+1/2), \tag{2.68}$$

$$w_i(n+1) = w_i(n+1/2) - 1/2\Delta\tau \left(\frac{\partial S}{\partial z_i}\right)^*\Big|_{z(n+1)} - 1/2\Delta\tau i V_i^\alpha(z(n+1))\lambda_2^\alpha. \tag{2.69}$$

$\lambda_1^\alpha, \lambda_2^\alpha$ are determined so that $z(n) \in \mathcal{J}_\sigma$ and $w(n) \in T_{z(n)}\mathcal{J}_\sigma$ are mapped to $z(n+1) \in \mathcal{J}_\sigma$ and $w(n+1) \in T_{z(n+1)}\mathcal{J}_\sigma$. $w_i(n+1/2)$ are not the tangent vectors but the vectors connecting $z_i(n)$ and $z_i(n+1)$. The constraint $z(n+1) \in \mathcal{J}_\sigma$ is represented by the equations,

$$\Phi_i(e(n+1), t(n+1)) - \tilde{z}_i = -1/2\Delta\tau^2 i V_i^\alpha(z(n))\lambda_1^\alpha, \tag{2.70}$$

where

$$\tilde{z}_i \coloneqq z_i(n) + \Delta\tau w_i(n) - 1/2\Delta\tau^2 \left(\frac{\partial S}{\partial z_i}\right)^*\Big|_{z(n)}. \tag{2.71}$$

The map $(z(n), w(n)) \to (z(n+1), w(n+1))$ is reversible for a small but finite step size $\Delta\tau$ so that a unique solution $(\lambda_1^\alpha, \lambda_2^\alpha)$ exists in Eqs. (2.67)-(2.69). Thus we need to take a small $\Delta\tau$ carefully. The solution $e(n+1), t(n+1), \lambda_1^\alpha$ is found by the fixed point

iteration method or Newton's method [15]. In these methods, we compute the sequence $(e_{(k)}, t_{(k)}, \lambda^{\alpha}_{1(k)})$ using the gradients,

$$\frac{\partial \Phi_i}{\partial e^{\alpha}}(e,t) = \varepsilon V_i^{\alpha}, \tag{2.72}$$

$$\frac{\partial \Phi_i}{\partial t}(e,t) = \left(\frac{\partial S}{\partial z_i}\right)^{*} = g^{\alpha} V_i^{\alpha}. \tag{2.73}$$

The flow direction e is represented by the linear combination of the tangent vectors $\{v_i^{\alpha}\}$ at the critical point as $e_i = e^{\alpha} v_i^{\alpha}$, where $e^{\alpha} \in \mathbb{R}$. The force term $(\partial S/\partial z_i)^{*}$ is a tangent vector and represented by the combination of the basis V_i^{α} with the coefficients $g^{\alpha} \in \mathbb{R}$. To derive the coefficients g^{α}, we need to compute the inverse matrix V^{-1} through the LU decomposition.

In the fixed point iteration method, we solve the following linear equation iteratively:

$$z_i^{(k)} - \tilde{z}_i + \frac{\partial \Phi_i}{\partial e^{\alpha}}(e(n), t(n)) \Delta e^{\alpha}_{(k)} + \frac{\partial \Phi_i}{\partial t}(e(n), t(n)) \Delta t_{(k)} = -1/2 \Delta \tau^2 i V_i^{\alpha}(z(n)) \lambda^{\alpha}_{1(k)}, \tag{2.74}$$

where $\Delta e^{\alpha}_{(k)}, \Delta t_{(k)}$ denote the increments, given by

$$\Delta e^{\alpha}_{(k)} = e^{\alpha}_{(k+1)} - e^{\alpha}_{(k)}, \tag{2.75}$$

$$\Delta t_{(k)} = t_{(k+1)} - t_{(k)}. \tag{2.76}$$

Since the flow direction e is a unit vector, we impose a constraint,

$$\sum_{\alpha=1}^{n} \Delta e^{\alpha}_{(k)} e^{\alpha}_{(k)} = 0. \tag{2.77}$$

Then the correction of the normalization $e^{\alpha}_{(k+1)} \to e^{\alpha}_{(k+1)} / \sqrt{1 + \|\Delta e_{(k)}\|^2}$ is the second order. Starting from the initial guess $z_j^{(0)} = \Phi_j(e_{(0)}, t_{(0)}) = z_j(n)$, we derive the sequence as follows:

$$\Delta t_{(k)} = -(g^{\alpha} e^{\alpha}_{(k)})^{-1} \mathrm{Re}\left[\left(V^{-1}(z(n))\right)_i^{\alpha} (z_i(n+1) - \tilde{z}_i) \right], \tag{2.78}$$

$$\Delta e^{\alpha}_{(k)} = -\varepsilon^{-1} \mathrm{Re}\left[\left(V^{-1}(z(n))\right)_i^{\alpha} (z_i(n+1) - \tilde{z}_i) \right] - \varepsilon^{-1} \Delta t_{(k)} g^{\alpha}, \tag{2.79}$$

$$e^{\alpha}_{(k+1)} = e^{\alpha}_{(k)} + \Delta e^{\alpha}_{(k)}, \tag{2.80}$$

$$t_{(k+1)} = t_{(k)} + \Delta t_{(k)}, \tag{2.81}$$

$$e^{\alpha}_{(k+1)} \to e^{\alpha}_{(k+1)} / \sqrt{1 + \|\Delta e_{(k)}\|^2}, \tag{2.82}$$

$$z_i^{(k+1)} = \Phi_i(e_{(k+1)}, t_{(k+1)}). \tag{2.83}$$

If the initial guess is sufficiently close to the solution, $z_i^{(k+1)}$ converges to $z_i(n+1)$ linearly, and the increments $\Delta e^\alpha_{(k)}, \Delta t_{(k)}$ decrease exponentially. We compute the sequence $(e_{(k)}, t_{(k)})$ until it satisfies the stopping condition,

$$\| V(z(n))^\alpha \left(\varepsilon \Delta e^\alpha_{(k)} + \Delta t g^\alpha \right) \|^2 < \epsilon'^2 \tag{2.84}$$

for a sufficiently small ϵ'^2 . After we obtain $e(n+1), t(n+1)$, we derive λ_1^α by the equation,

$$1/2\Delta\tau^2 \lambda_1^\alpha = \mathrm{Im} \left[\left(V^{-1}(z(n)) \right)^\alpha_i \left(z_i(n+1) - \tilde{z}_i \right) \right]. \tag{2.85}$$

In Newton's method, we find the solution $e(n+1), t(n+1), \lambda_1^\alpha$ as follows. We define the function,

$$F = (F_I) = \begin{pmatrix} \Phi_i(e,t) - \tilde{z}_i + 1/2\Delta\tau^2 i V_i^\alpha(z(n)) \lambda_1^\alpha \\ e^\alpha e^\alpha - 1 \end{pmatrix}, \tag{2.86}$$

and the variables,

$$W = (W^A) = \begin{pmatrix} e^\alpha \\ t \\ \lambda_1^\alpha \end{pmatrix}, \tag{2.87}$$

where $I = 1, \ldots, n+1$ and $A = 1, \ldots, n+1$. Then the constraints are represented as

$$F_I(W^A) = 0. \tag{2.88}$$

The equations (2.88) are solved by generating the sequence $W_{(k)}$ according to the linear equations:

$$\frac{\partial F_I}{\partial W^A}(W_{(k)}) \Delta W^A_{(k)} = -F_I(W_{(k)}), \tag{2.89}$$

where

$$\Delta W^A_{(k)} = W^A_{(k+1)} - W^A_{(k)}. \tag{2.90}$$

We can write the explicit form of the linear equations (2.89) as

$$\begin{pmatrix} \varepsilon V_i^{\alpha(k)} & g^\beta V_i^{\beta(k)} & i V_i^{\alpha(0)} \end{pmatrix} \begin{pmatrix} \Delta e^\alpha_{(k)} \\ \Delta t_{(k)} \\ \Delta \lambda^\alpha_{1(k)} \end{pmatrix} = -\Phi_i(e_{(k)}, t_{(k)}) + \tilde{z}_i - 1/2\Delta\tau^2 i V_i^{\alpha(0)} \lambda^\alpha_{1(k)}, \tag{2.91}$$

and

$$2 e^\alpha_{(k)} \Delta e^\alpha_{(k)} = -e^\alpha_{(k)} e^\alpha_{(k)} + 1, \tag{2.92}$$

where $\{V_i^{\alpha(k)}\}$ is the basis of the tangent vectors at $z^{(k)}$. Starting from the initial guess,

$z_j^{(0)} = \Phi_j(e_{(0)}, t_{(0)}) = z_j(n)$ and $\lambda_{1(0)}^{\alpha} = 0$, we derive the sequence as follows:

$$\Delta W_{(k)}^A = -\left[\left(\frac{\partial F}{\partial W}\right)^{-1}\right]_I^A F_I(W_{(k)}), \tag{2.93}$$

$$W_{(k+1)}^A = W_{(k)}^A + \Delta W_{(k)}^A, \tag{2.94}$$

$$z_i^{(k+1)} = \Phi_i(e^{(k+1)}, t^{(k+1)}), \tag{2.95}$$

$$V_i^{\alpha(k+1)} = \Psi_i^{\alpha}(e^{(k+1)}, t^{(k+1)}), \tag{2.96}$$

where Ψ_i^{α} is the map given by the flow (2.27) of the initial tangent vector $V_i^{\alpha}(0) = v_i^{\alpha}$ along the flow of $z = \Phi(e, t)$.

If the initial guess is sufficiently close to the solution, $z_i^{(k+1)}$ converges to $z_i(n+1)$ quadratically. The stoppoing condition is given by

$$\mathrm{Re}(F_I^* F_I) < \epsilon'^2, \tag{2.97}$$

with a sufficiently small ϵ'^2.

In the fixed point iteration method, we use the gradients at the initial guess through the iteration and we can save the iterative computation of the tangent vectors. In Newton's method, though we need to compute the tangent vectors iteratively, we can find the solution for the larger distance between the initial guess and the solution.

Once we obtain $e(n+1), t(n+1)$, we compute the tangent vectors $V_i^{\alpha}(z(n+1)) = \Psi_i^{\alpha}(e(n+1), t(n+1))$, which is already done in Newton's method, and compute the inverse matrix $V^{-1}(z(n+1))$. Then to satisfy the constraint $w(n+1) \in T_{z(n+1)}\mathcal{J}_\sigma$, we determine λ_2^{α} as

$$1/2\Delta\tau\lambda_2^{\alpha} = \mathrm{Im}\left[\left(V^{-1}(z(n+1))\right)_i^{\alpha}\left(w_i(n+1/2) - 1/2\Delta\tau\left(\frac{\partial S}{\partial z_i}\right)^*\Big|_{z(n+1)}\right)\right]. \tag{2.98}$$

2.3.3 Hybrid Monte Carlo on Lefschetz thimble

Now we summarize the hybrid Monte Carlo update on the Lefschetz thimble $\mathcal{J}_\sigma$.

1. Set the initial configuration (e, t) and compute

$$z_i = \Phi_i(e, t), \quad V_i^{\alpha} = \Psi_i^{\alpha}(e, t) \tag{2.99}$$

by the Runge-Kutta method. Also compute V^{-1} by the LU decomposition. Here $\Phi_i(e, t)$ is the solution of Eq. (2.27) at the flow time t with the initial condition $z_i(0) = z_\sigma + \varepsilon e_i$, where z_σ is a critical point and ε is a small positive constant. Similarly, $\Psi_i^{\alpha}(e, t)$ is the solution of Eq. (2.47) at the flow time t with the initial condition $V_i^{\alpha}(0) = v_i^{\alpha}$, where v_i^{α} is the tangent vectors at the critical point z_σ and is given by Eq. (2.45).

2. Generate n pairs of unit Gaussian random numbers $\xi_i, \eta_i\,(i = 1, \ldots, n)$. Then the tentative momenta $w_i = \xi_i + i\eta_i$ are projected on the tangent space $T_z\mathcal{J}_\sigma$ by

$$w_i = V_i^\alpha \mathrm{Re}\left[(V^{-1})_j^\alpha w_j\right]. \tag{2.100}$$

3. Iteratively compute the discretized molecular dynamics (2.67)-(2.69) with the constraints $z(n) \in \mathcal{J}_\sigma$ and $w(n) \in T_{z(n)}\mathcal{J}_\sigma$, using the fixed point iteration method or Newton's method. At each step in Eqs. (2.67)-(2.69), we compute the tangent vectors V and the inverse matrix V^{-1}. At the final step in Eqs. (2.67)-(2.69), we have (z', w').

4. Accept the proposed configuration (w', z') by the probability $\min\{1, e^{-\Delta H}\}$, where $\Delta H = H(w', z') - H(w, z)$.

2.3.4 Residual phase

To evaluate the integral over the thimble $\mathcal{J}_\sigma$, we introduce the real orthogonal coordinate in the vicinity of a point z. The basis of the tangent vectors $\{V_i^\alpha\}$ can be orthonormalized by the QR decomposition such as Gram-Schmidt orthonormalization,

$$V_i^\alpha = Q_i^\beta R^{\beta\alpha}, \tag{2.101}$$

where $\{Q_i^\alpha\}$ is a basis satisfying $\mathrm{Re}Q_i^{\alpha *}Q_i^\beta = \delta^{\alpha\beta}$, and $R^{\alpha\beta}$ is a real upper triangle matrix. From the reality condition (2.48), we have $\mathrm{Im}Q_i^{\alpha *}Q_i^\beta = 0$. Thus Q is a unitary matrix. The tangent vector is represented as the linear combination of Q_i^α and the point in the vicinity of z is parametrized as $\delta z_i = Q_i^\alpha \delta\xi^\alpha$. Thus the complex measure is expressed as $d^n z = d^n\xi e^{i\varphi(z)}$, where $e^{i\varphi(z)} \coloneqq \det Q = \det V/|\det V|$. The determinant $\det V$ is computed through LU decomposition, in which we can also compute the inverse V^{-1}. We note that the hybrid Monte Carlo on the thimble generates the configurations according to the probability proportional to $e^{-\mathrm{Re}(S(z))}$ and the measure is given by $|d^n z| \coloneqq d^n\xi$. Thus the average of an observable $O(z)$ gives the following integral:

$$\frac{1}{Z'_\sigma}\int |d^n z|\, e^{-\mathrm{Re}(S(z))}O(z) \approx \frac{1}{N_{\mathrm{conf}}}\sum_{k=1}^{N_{\mathrm{conf}}} O(z^{(k)}), \tag{2.102}$$

where

$$Z'_\sigma = \int |d^n z|\, e^{-\mathrm{Re}(S(z))}. \tag{2.103}$$

Here, $z^{(k)}\,(k = 1, \ldots, N_{\mathrm{conf}})$ denote the measured configurations, which are sampled from the sequence generated by the hybrid Monte Carlo update with sufficiently large intervals so that the autocorrelation is negligible. Therefore to evaluate the expectation value of

an observable O over the thimble $\mathcal{J}_\sigma$, we need to include the residual phase factor $e^{i\varphi(z)}$ in the observable as follows:

$$\langle O \rangle_{\mathcal{J}_\sigma} \approx \frac{N_{\rm conf}^{-1} \sum_k e^{i\varphi(z^{(k)})} O(z^{(k)})}{N_{\rm conf}^{-1} \sum_k e^{i\varphi(z^{(k)})}}. \tag{2.104}$$

As we discussed that reweighting procedure (2.7) does not work practically if the phase is oscillatory, the average of the residual phase factor $e^{i\varphi(z)}$ need to be sufficiently large so that the evaluation (2.104) is valid numerically. The matrix Q is written by

$$(Q_i^1, \ldots, Q_i^n) P^T = (e^{i\theta_1} u_i^1, \ldots, e^{i\theta_n} u_i^n), \tag{2.105}$$

where P is an orthogonal matrix, and $\{u_i^\alpha\}$ is an orthonormal basis of real vectors.The residual phase represents the total phase $e^{i\varphi(z)} = e^{i\sum_j \theta_j}$ between the tangent vectors on the thimble $\mathcal{J}_\sigma$ and the real space $\mathbb{R}^n$. If the shape of the integration contour changes rapidly, the cancellation between the positive and negative contribution may happen. Thus we need to examine the residual phase carefully when we use the hybrid Monte Carlo update on the thimble.

2.3.5 Computational cost

The computational cost of solving the gradient flow equation (2.27) using the Runge-Kutta method is $\mathcal{O}(n)$ and $\mathcal{O}(n^2)$ for the configuration z_i and the basis of tangent vectors $\{V_i^\alpha(z)\}$, which are parametrized by the flow direction e and the flow time t. The computational cost of deriving the determinant $\det V(z)$ and inverse $V^{-1}(z)$ using the LU decomposition is $\mathcal{O}(n^3)$. In the lattice model the number of the degrees of freedom is proportional to the volume size V. Therefore the total computational cost of the hybrid MonteCarlo update is $\mathcal{O}(V^3)$.

Chapter 3

Generalized Lefschetz thimble method

In general, models in quantum field theories are very complicated to analyze the critical points and the thimble which contribute to the path integral. Moreover, fermionic models, for example lattice QCD with the finite chemical potential have fermion determinants after the fermions are integrated out, and generally the determinants contain many zeros. Since these zeros are connected by the end points of Lefschetz thimbles, we expect that many Lefschetz thimbles contribute to the path integrals. For example, in one-dimensional massive Thirring model at finite density, which is the solvable toy model of a fermionic system, the Monte Carlo simulation on the single dominant thimble gives an incorrect answer because the contribution of subdominant Lefschetz thimbles is not negligible [40, 41]. Thus Monte Carlo approaches on a Lefschetz thimble do not seem to work well. One of the approaches to avoid these problems may be provided by the alternative deformed contour which is the connected space and on which the sign problem is mild. This approach is called the Generalized Lefschetz thimble method [12].

3.1 Flow of the original contour

In this section, we consider the integration contour deformed by the gradient flow. we discuss the behavior of the flowed contour by the gradient flow. Using a simple one-dimensional integral, we view that the flowed contour approaches Lefshets thimbles which contribute to the path integral.

3.1.1 Behavior of the flowed contour

So far we have used the gradient flow (2.27) to construct the thimbles. As explained previously, we first find the critical point which contributes to the path integral, and

then the thimbles are parametrized by flowing the points in the vicinity of the critical point. Now, we consider each point on the original contour $\mathcal{C}_{\mathbb{R}}$ as an initial condition of the gradient flow, and flow the original contour $\mathcal{C}_{\mathbb{R}}$ up to a finite time T_{flow}. Let us call the flowed contour $\mathcal{C}(T_{\text{flow}})$. Since the real part of the action grows monotonically as the flow time increases, the absolute value of the integrand on the flowed contour is smaller than that on the original contour. Thus the integral over the flowed contour is convergent for any flow time T_{flow}. If a thimble $\mathcal{J}_\sigma$ contributes to the path integral, the dual thimble $\mathcal{K}_\sigma$ intersect with the original contour $\mathcal{C}_{\mathbb{R}}$ on a point x_σ. The point in the vicinity of the intersection point x_σ flows toward the critical point z_σ, and then deviates from it along the thimble $\mathcal{J}_\sigma$. Thus by the gradient flow, the region on $\mathcal{C}_{\mathbb{R}}$ lying in the vicinity of the intersection point x_σ approaches the critical point z_σ, and then covers the thimble $\mathcal{J}_\sigma$ as the flow time increases. On the other hand, the points far from the intersection points quickly go to the regions where the action diverges, that is, the infinity or the zeros of the fermion determinant. Therefore, as the flow time goes to infinity, the flowed contour $\mathcal{C}(T_{\text{flow}})$ converges to the thimbles which are homologically equivalent to the original contour:

$$\lim_{t\to\infty} \mathcal{C}(t) = \sum_{\sigma\in\Sigma} n_\sigma \mathcal{J}_\sigma, \tag{3.1}$$

where n_σ is the intersection number given by $n_\sigma = \langle \mathcal{C}_{\mathbb{R}}, \mathcal{K}_\sigma \rangle$. Since the small regions in the vicinity of the intersection points contribute to the path integral, the fluctuation of the phase $\exp(-i\text{Im}S)$ is small. Generally the phases on the different critical points are different, and the phase variation occurs when the flowed contour crosses the regions where the real part of the action $\exp(-\text{Re}S)$ is extremely large. The relative phases among the critical points may cancel, but we expect that such a cancellation happens by approximate symmetries. Then it is avoided by adding a symmetry-breaking term $\varepsilon S_{SB}(z)$ and the physical results are obtained by extrapolating to $\varepsilon \to 0$. Therefore we expect the sign problem on the flowed contour is mild.

3.1.2 Flow contour in an example

The flow of the integration contour is explicitly viewed by a simple example. Let us consider the one-dimensional integral given by

$$Z = \int_\infty^\infty d\phi\, (\phi - \phi_1)(\phi - \phi_2) e^{-\phi^2/(2\sigma)}. \tag{3.2}$$

The effective action is given by $S(\phi) = \phi^2/(2\sigma) - \log[(\phi - \phi_1)(\phi - \phi_2)]$. It may be considered as a toy model of a fermionic system coupled to an auxiliary field ϕ, where the fermionic field is integrated out and the fermion determinant appears as the polynomial $(\phi - \phi_1)(\phi - \phi_2)$. Fig. 3.1 shows the thimbles, the dual thimbles, the critical points, the zeros, and the flowed contour. There are four regions where the action diverges: two

asymptotic regions with $\mathrm{Re}(\phi^2/(2\sigma)) > 0$, and two zeros. The thimbles connect with the two of those regions. For $\sigma = 0.5, \phi_1 = i - 1, \phi_2 = 2i + 1$, two dual thimbles intersect with the original contour. Thus, the linear combination of two thimbles accompanied by those dual thimbles is homologically equivalent to the original contour $\mathbb{R}$. As shown in Fig. 3.1, the flowed contour approaches those thimbles. We can view that the regions in the vicinities of the intersection points approach the critical points, and then expand along the thimbles. The phase $\exp(-\mathrm{Im}S)$ varies slowly with the value close to that on the thimble nearby, but drastically changes when the flowed contour passes by the zero which connects the two thimbles.

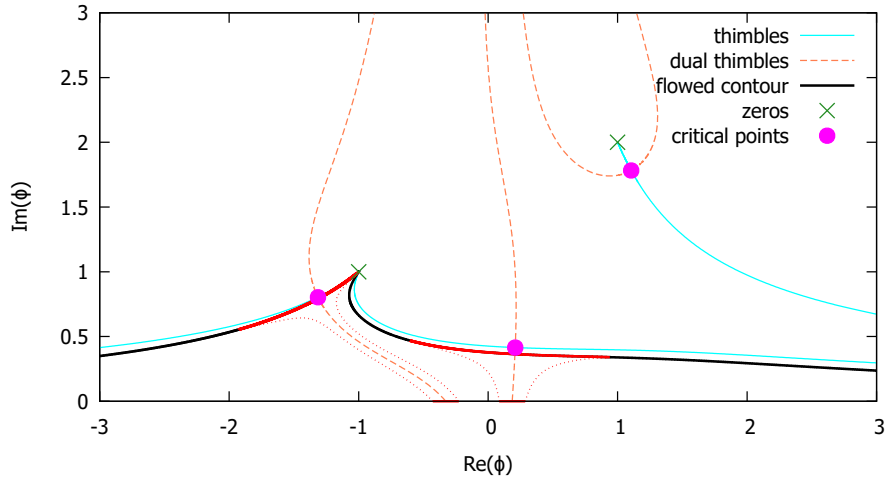

Figure 3.1: Thimbles (solid cyan lines), dual thimbles (dashed coral lines), critical points (magenta blobs), zeros (green crosses), and a flowed contour (solid black line) are shown for $\sigma = 0.5, \phi_1 = i - 1, \phi_2 = 2i + 1$ and $T_{\mathrm{flow}} = 1$. Also the flows of the real regions in the vicinities of the points intersecting with the dual thimbles are shown (red lines).

3.2 Algorithm on the flowed contour

In this section we explain two algorithms in which we evaluate path integrals on the flowed contour. We first consider the Metropolis method with the real variables, where the update requires $\mathcal{O}(n^2)$ computation. The distribution of the proposed configuration on the flowed contour is anisotropic, and the sampling is inefficient. However, this method has the advantage that we are free from solving an iterative method such as the fixed point iteration method and Newton's method. We then consider the hybrid Monte Carlo method on the flowed contour. In this method, we need to solve an iterative method,

where we may not find a solution for a large step size. However, this method provides configurations efficiently.

3.2.1 Simulation using the real configuration space

We may carefully adjust the flow time so that the flowed contour does not approach the regions where the action diverges but that the sign problem is mild. Then we can implement hybrid Monte Carlo algorithm on the flowed contour $\mathcal{C}(T_{\text{flow}})$ in the same way as that on the Lefschetz thimble. However, on the flowed contour we need to solve Newton's method iteratively to propose next configurations. We can rewrite the path integral using the real configuration space, instead of the curved space $\mathcal{C}(T_{\text{flow}})$. Since the map $\Phi_{T_{\text{flow}}} : \mathcal{C}_{\mathbb{R}} \to \mathcal{C}(T_{\text{flow}})$ by the gradient flow (2.27) is a diffeomorphism, we can change the integration variables $z \in \mathcal{C}(T_{\text{flow}})$ back to the real variables $x \in \mathcal{C}_{\mathbb{R}}$. Thus we have

$$\begin{aligned} Z = \int_{\mathcal{C}_{\mathbb{R}}} d^n x \, \exp(-S(x)) &= \int_{\mathcal{C}(T_{\text{flow}})} d^n z \exp(-S(z)) \\ &= \int_{\mathcal{C}_{\mathbb{R}}} d^n x \, \det V(T_{\text{flow}}, x) \exp(-S(\Phi_{T_{\text{flow}}}(x))), \end{aligned} \tag{3.3}$$

where $V(T_{\text{flow}}, x)$ is the Jacobian matrix $V_i^\alpha(T_{\text{flow}}, x) = \partial(\Phi_{T_{\text{flow}}})_i / \partial x^\alpha$, and also represents the basis of the tangent vectors on the flowed point $z = \Phi_{T_{\text{flow}}}(x)$. $V(T_{\text{flow}}, x)$ is computed by the differential equation (2.47), and the initial condition is a unit matrix as $V(0, x)_i^\alpha = \delta_i^\alpha$ [1)] . The initial condition $V(0, x)_i^\alpha$ is independent of x since the original contour $\mathcal{C}_{\mathbb{R}}$ is a hyperplane. We note that the phase fluctuation of the integrand in the second line of Eq. (3.3) is milder than the original integrand. Thus we may numerically evaluate the path integral directly on the real space $C_{\mathbb{R}}$. Then the expectation value of an observable O is given by

$$\langle O \rangle = \frac{\langle e^{i\varphi} O \rangle_{S_{\text{eff}}}}{\langle e^{i\varphi} \rangle_{S_{\text{eff}}}}. \tag{3.4}$$

Here

$$\varphi(x, T_{\text{flow}}) = \arg \det V(T_{\text{flow}}, x) - \text{Im} S(\Phi_{T_{\text{flow}}}(x)) \tag{3.5}$$

is the phase coming from the Jacobian determinant and the action, and

$$\langle O \rangle_{S_{\text{eff}}} = \int_{\mathcal{C}_{\mathbb{R}}} d^n x \, e^{-S_{\text{eff}}(x, T_{\text{flow}})} O(\Phi_{T_{\text{flow}}}(x))) \tag{3.6}$$

is the expectation value of the observable O with the action,

$$S_{\text{eff}}(x, T_{\text{flow}}) = \text{Re} S(\Phi_{T_{\text{flow}}}(x)) - \log \left| \det V(T_{\text{flow}}, x) \right| . \tag{3.7}$$

[1)] We note that originally in Eq. (2.47) we start from the vicinity of a critical point and consider the flow along the thimble, but now we start from the point on the real space and consider the flow of the real space.

3.2.2 Grady algorithm

Here we consider the Metropolis algorithm using Eq. (3.6). Naively this algorithm is given by the following procedure. We set the initial condition as x, and propose a configuration $x' = x + \Delta x$ according to the distribution function $\Pr(\Delta x)$, which we assume to be isotropic, for example, the Gaussian distribution. The Metropolis test may be simply given by the acceptance ratio,

$$P_{\rm acc}(x \to x') = \min\{1, e^{-\Delta S_{\rm eff}}\}, \tag{3.8}$$

where $\Delta S_{\rm eff}$ is the variation of the action given by

$$\Delta S_{\rm eff} = S_{\rm eff}(x', T_{\rm flow}) - S_{\rm eff}(x, T_{\rm flow}). \tag{3.9}$$

We note that this update satisfies the detailed balance condition (2.6), since the distribution function $\Pr(\Delta x)$ is explicitly symmetric under the exchange of x and x'. For each update, we need to compute the gradient flow equation, and the computational cost is $O(n)$. However we also need to compute the Jacobian determinant, and the computational cost is $O(n^3)$.

In Ref. [35] an algorithm which avoids computing the Jacobian determinant is introduced based on the Grady algorithm [42] as follows. To propose a configuration x', we generate random numbers $\eta_i^{(R)}, \eta_i^{(I)}$ according to the distribution proportional to $\exp[-\eta_i^{(R)}\eta_i^{(R)}/\delta^2]$ and $\exp[-\eta_i^{(I)}\eta_i^{(I)}/\delta^2]$. Here δ is a parameter indicating the step size, and is adjusted so that the acceptance rate is sufficiently large. We may consider the complex vector $\eta_i = \eta_i^{(R)} + i\eta_i^{(I)}$ as the distribution around the flowed point $z = \Phi_{T_{\rm flow}}(x)$. Then after projecting η_i on the tangent space at z, we can relate it to the tangent space at x as $\Delta x = \mathrm{Re}(\,(V^{-1})|_x\,\eta)$, and propose a configuration $x' = x + \Delta x$. The proposal is isotropic on the flowed contour if we take the step size sufficiently small so that the map of the neighborhood of x onto the flowed contour $C(T_{\rm flow})$ is linearized. Since the set of complex vectors $\{V_i^\alpha\}$ and $\{iV_i^\alpha\}$ spans $\mathbb{C}^n$ with real coefficients, we have

$$\eta_i = V_i^\alpha c_\parallel^\alpha + iV_i^\beta c_\perp^\beta, \quad c_\parallel^\alpha, c_\perp^\beta \in \mathbb{R}. \tag{3.10}$$

The measure is transformed as

$$\prod_i d\eta_i^{(R)} d\eta_i^{(I)} = \det(V^\dagger V) \prod_\alpha dc_\parallel^\alpha dc_\perp^\alpha. \tag{3.11}$$

Thus the proposal distribution is given by

$$\Pr(x \to x') = \sqrt{\frac{\det\,(V^\dagger V)|_x}{\pi^n \delta^2}} \exp\left[-\Delta x^T\,(V^\dagger V)\big|_x\,\Delta x/\delta^2\right]. \tag{3.12}$$

We note that the matrix $V^\dagger V$ is real, since the reality condition (2.48) holds. To compute the acceptance ratio, we generate the complex vector $\zeta_i = \zeta_i^{(R)} + i\zeta_i^{(I)}$ according to the

distribution proportional to $\exp[-\zeta_i^{(R)}\zeta_i^{(R)}]$ and $\exp[-\zeta_i^{(I)}\zeta_i^{(I)}]$. Then we introduce an auxiliary complex vector ξ, which is given by $\xi = (V^{-1})|_{x'}\,\zeta$. The distribution of ξ is given by

$$P_{\rm aux}(\xi) = \frac{\det\,(V^\dagger V)\big|_{x'}}{\pi^n}\exp\left[-\xi^\dagger\,(V^\dagger V)\big|_{x'}\,\xi\right], \tag{3.13}$$

and we accept the proposal by the probability,

$$P_{\rm acc} = \min\left\{1, \exp[-{\rm Re}\Delta S + \xi^\dagger(\Delta V^2)\xi - \Delta x^T(\Delta V^2)\Delta x/\delta^2]\right\}, \tag{3.14}$$

where $\Delta S = S(\Phi_{T_{\rm flow}}(x')) - S(\Phi_{T_{\rm flow}}(x))$, and

$$(\Delta V^2)^{\alpha\beta} = V_i^{\alpha *}(x', T_{\rm flow})V_i^\beta(x', T_{\rm flow}) - V_i^{\alpha *}(x, T_{\rm flow})V_i^\beta(x, T_{\rm flow}). \tag{3.15}$$

The total transition probability is given by

$$T(x\to x') = {\rm Pr}(x\to x')\int d^n\xi^{(R)}d^n\xi^{(I)}\,P_{\rm aux}(\xi)P_{\rm acc}, \tag{3.16}$$

where the measure is defined by $d^n\xi^{(R)}d^n\xi^{(I)} = \prod_i d\xi_i^{(R)}d\xi_i^{(I)}$. Then we have

$$\begin{aligned} &e^{-S_{\rm eff}(x,T_{\rm flow})}T(x\to x') \\ &\quad = \frac{\det\,(V^\dagger V)\big|_x\,\det\,(V^\dagger V)\big|_{x'}}{\pi^{3n/2}\delta}\int d^n\xi^{(R)}d^n\xi^{(I)}\,\min\left\{e^{-F(x,x')}, e^{-F(x',x)}\right\}, \end{aligned} \tag{3.17}$$

where

$$F(x,x') = S(\Phi_{T_{\rm flow}}(x)) + \Delta x^T\,(V^\dagger V)\big|_x\,\Delta x/\delta^2 + \xi^\dagger\,(V^\dagger V)\big|_{x'}\,\xi. \tag{3.18}$$

Therefore, the detailed balance condition (2.6) is satisfied.

Now we summarize the generalized thimble method using the Metropolis algorithm on the real space.

1. Set the initial configuration $x \in \mathcal{C}_{\mathbb{R}}$.
2. Generate a complex vector $\eta \in \mathbb{C}^n$ according to the distribution proportional to $\exp[-\eta^\dagger\eta/\delta^2]$.
3. Compute $\Delta x = {\rm Re}\,(V^{-1})|_x\,\eta$, and propose a configuration $x' = x + \Delta x$.
4. Generate a complex vector $\zeta \in \mathbb{C}^n$ according to the distribution proportional to $\exp[-\zeta^\dagger\zeta]$.
5. Compute $\xi = (V^{-1})|_{x'}\,\zeta$ and accept the proposed configuration x' by the probability $P_{\rm acc}$.

In step 3 and 5, Δx and ξ are computed using an iterative method. In this method, V^{-1} is not explicitly computed, but $V\rho$ is iteratively computed for complex vectors $\rho = \rho^{(R)} + i\rho^{(I)}$. $V\rho$ is computed by flowing the initial vector $V(0)\rho^{(R)}$ and $V(0)\rho^{(I)}$ according to Eq. (2.47), and thus the computational cost is $\mathcal{O}(n)$. To compute the expectation value (3.6), we need to compute the phase $e^{i\varphi}$. It requires the computation scaling as $\mathcal{O}(n^3)$, but the set of the sampled configurations is a small subset of the sequence generated by the Metropolis update. Thus the computational cost of the phase is relatively small. In addition, an efficient method to compute the phase is proposed in Ref. [43].

3.2.3 Hybrid Monte Carlo on the flowed contour

Now we consider the hybrid Monte Carlo algorithm on the flowed contour using the gradient flow. Here, the molecular dynamics on the flowed contour Σ is given by

$$\frac{dz_i}{d\tau} = w_i, \tag{3.19}$$

$$\frac{dw_i}{d\tau} = -\left(\frac{\partial S}{\partial z_i}\right)^* - iV_i^\alpha \lambda^\alpha, \tag{3.20}$$

where $\lambda^\alpha \in \mathbb{R}$ are the Lagrange multipliers.

z_i is constrained on the flowed contour Σ and w_i is constrained on the tangent space $T_z\Sigma$. the conserved Hamiltonian is given by

$$H = \frac{1}{2} w_i^* w_i + \mathrm{Re}[S(z)], \tag{3.21}$$

since

$$\frac{dH}{d\tau} = -\mathrm{Re}(w_i^* V_i^\alpha)\lambda^\alpha = 0. \tag{3.22}$$

Eqs. (3.19) and (3.20) are discretized as follows:

$$w_i(n+1/2) = w_i(n) - 1/2\Delta\tau \left(\frac{\partial S}{\partial z_i}\right)^*\Big|_{z(n)} - 1/2\Delta\tau i V_i^\alpha(z(n))\lambda_1^\alpha, \tag{3.23}$$

$$z_i(n+1) = z_i(n) + \Delta\tau w_i(n+1/2), \tag{3.24}$$

$$w_i(n+1) = w_i(n+1/2) - 1/2\Delta\tau \left(\frac{\partial S}{\partial z_i}\right)^*\Big|_{z(n+1)} - 1/2\Delta\tau i V_i^\alpha(z(n+1))\lambda_2^\alpha, \tag{3.25}$$

where $\lambda_1^\alpha, \lambda_2^\alpha$ are determined so that $z(n+1) \in \Sigma$ and $w(n+1) \in T_z\Sigma$.

We may use the fixed point iteration method or Newton's method to solve the equations. In these methods we set an initial guess $(z_j^{(0)}, \lambda_{1(0)}^\alpha) = (z_j(n), 0)$, and generate a sequence $(z_j^{(k)}, \lambda_{1(k)}^\alpha)$. Then the solution $(z_j(n+1), \lambda_1^\alpha)$ is obtained by the limit of the sequence, if the step size $\Delta\tau$ is sufficiently small. Here we define

$$\tilde{z}_i \coloneqq z_i(n) + \Delta s w_i(n) - 1/2(\Delta s)^2(\partial_i S(z(n)))^*. \tag{3.26}$$

In the fixed point iteration method, we obtain the solution $z(n+1)$ by solving the recurrence relation,

$$\Delta x_\alpha^{(k+1)} = -\mathrm{Re}[(V^{-1})_j^\alpha (z_j^{(k)} - \tilde{z}_j)], \tag{3.27}$$

$$x_\alpha^{(k+1)} = x_\alpha^{(k)} + \Delta x_\alpha^{(k+1)}, \tag{3.28}$$

$$z_i^{(k+1)} = \Phi_i[x^{(k+1)}], \tag{3.29}$$

where Φ_i is the map flowing the initial point $x \in \mathcal{C}_\mathbb{R}$ to the point $z \in \Sigma$.

In Newton's method, we obtain the solution $(z(n+1), \lambda)$ by solving the recurrence relation,

$$\begin{pmatrix} \Delta x^{(k+1)} \\ \Delta\lambda_{1(k+1)} \end{pmatrix} = \begin{pmatrix} V^{(k)} & iV^{(0)} \end{pmatrix}^{-1} (-z_i^{(k)} + \tilde{z} - iV^{(0)\alpha}\lambda_{1(k)}^\alpha), \tag{3.30}$$

$$x^{(k+1)} = x^{(k)} + \Delta x^{(k+1)}, \tag{3.31}$$

$$z^{(k+1)} = \Phi[x^{(k+1)}], \tag{3.32}$$

$$V^{(k+1)} = \Psi[x^{(k+1)}], \tag{3.33}$$

$$\lambda_{1(k)} = \lambda_{1(k)} + \Delta\lambda_{1(k+1)}, \tag{3.34}$$

where Ψ_i^α is the map flowing the initial tangent vector δ_i^α at $x \in \mathcal{C}_\mathbb{R}$ to the tangent vector $V_i^\alpha \in T_z\Sigma$.

After obtaining the solution $(z(n+1), \lambda_1^\alpha)$, we compute the inverse of the tangent vectors $V_i^\alpha(z(n+1))$. Since $w_i(n+1)$ is constrained on the tangent space $T_{z(n+1)}\Sigma$, we have

$$w_i(n+1) = V_i^\alpha|_{z(n+1)}\, \mathrm{Re}\left[(V^{-1})_j^\alpha\big|_{z(n+1)}\, \tilde{w}_i(n+1) \right], \tag{3.35}$$

where

$$\tilde{w}_i(n+1) = w_j(n+1/2) - 1/2\Delta\tau \left(\frac{\partial S}{\partial z_j} \right)^* \Bigg|_{z(n+1)}. \tag{3.36}$$

The hybrid Monte Carlo update on the flowed contour using the gradient flow is given as follows:

1. Set the initial configuration x_i and compute

$$z_i = \Phi_i(x), \quad V_i^\alpha = \Psi_i^\alpha(x) \tag{3.37}$$

by the Runge-Kutta method. Also compute the inverse of the tangent vectors V_i^α. Here $\Phi_i(x)$ is the solution of Eq. (2.27) at the flow time T_{flow} with the initial condition $z_i(0) = x_i$. Similarly, $\Psi_i^\alpha(x)$ is the solution of Eq. (2.47) at the flow time T_{flow} with the initial condition $V_i^\alpha(0) = \delta_i^\alpha$.

2. Generate n pairs of unit Gaussian random numbers $\xi_i, \eta_i\,(i = 1, \ldots, n)$. Then the tentative momenta $w_i = \xi_i + i\eta_i$ are projected on the tangent space $T_z\Sigma$ by

$$w_i = V_i^{\alpha}\mathrm{Re}((V^{-1})_j^{\alpha} w_j). \tag{3.38}$$

3. Iteratively compute the discretized molecular dynamics (3.23)-(3.25) using the fixed point iteration method or Newton's method. In Eqs. (3.23)-(3.25), we update $z_i = \Phi_i(x)$, $V_i^{\alpha} = \Psi_i^{\alpha}(x)$ and the inverse of the tangent vectors V^{-1}.

4. Accept the proposed configuration (w', z') by the probability $\min\{1, e^{-\Delta H}\}$, where $\Delta H = H(w', z') - H(w, z)$.

Chapter 4

Gradient flows without blow-up

In chapter 2, we introduced the gradient flow equation,

$$\frac{d}{dt}z_i(t) = \left(\frac{\partial S}{\partial z_i}\right)^* . \tag{4.1}$$

Once we specify the critical points, using the gradient flow we can find the associated Lefschetz thimbles, on which the imaginary parts of the actions are constant. Also in the generalized Lefschetz thimble method, we can deform the integration contour so that the phase fluctuations are mild. Thus the gradient flow (4.1) may be useful to solve the sign problem. However, as the flow time increases, the deformed contour is divided by the regions where the real part of the action is significantly large. Then the sequence of the Monte Carlo update is trapped to a limited region in the deformed contour, and the situation is the same as in the simulation on a single thimble. Moreover, as we show later, the deformed contour goes to infinity or zeros of the fermion determinant in a finite flow time, and the force term $(\partial S/\partial z_i)^*$ of the gradient flow equation (4.1) diverges. Here we call this phenomenon the blow-up. To circumvent these problems, We need to tune the flow time carefully, but finding such a flow time may not be practical. In Ref. [26], new gradient flows are proposed to avoid the blow-up. In this chapter we review the proposal.

4.1 Blow-up problem

In this section, we show that the blow-up of the gradient flow is caused by both the bosonic action and the fermion determinant, using simple toy models. The blow-up is a generic phenomenon for non-linear differential equations, and also seen in lattice models as discussed in Chapter 5 using the Thirring model.

4.1.1 Blow-up of bosonic action

Let us consider the following example:

$$Z = \int_{-\infty}^{\infty} dx\, e^{-\frac{\lambda}{4}x^4}. \tag{4.2}$$

The action is given by $S(x) = (\lambda/4)x^4$, and may be considered as a toy model of a massless scalar field theory. The gradient flow (4.1) is written as

$$\frac{d}{dt}x(t) = \lambda x^3. \tag{4.3}$$

Here we consider a real initial condition $x(0) = x_0 > 0$. Then the force term $(\partial S/\partial x)^*$ is real, and x is real for any flow time t. We can solve the differential equation (4.3) analytically, and obtain

$$x(t) = \frac{1}{\sqrt{x_0^{-2} - 2\lambda t}}. \tag{4.4}$$

Explicitly the solution blows up as t approaches $1/(2\lambda x_0^2)$.

More generally, let us consider the action is a multivariable polynomial function of degree k with the variables $z_i \in \mathbb{C}^n$. From the inequality (2.30), the real part of the action goes to infinity as the flow time increases. Thus $r = \sqrt{z_i^* z_i}$ also goes to infinity, and behaves as

$$\frac{d}{dt}r \approx cr^{k-1}, \tag{4.5}$$

where c is a positive constant. If the degree k is larger than two, the asymptotic behavior is given as $r \approx \kappa(t_c - t)^{-1/(k-2)}$, where κ is a positive constant and t_c is a blow-up time. Exceptionally if $k = 2$, the asymptotic behavior is given as $r \approx r_0 e^{ct}$ with a positive constant r_0.

4.1.2 Blow-up of fermion determinant

Next, let us consider the following example:

$$Z = \int_{-\infty}^{\infty} dx\, (1 - x^2)e^{-x^2}. \tag{4.6}$$

The action is given by $S(x) = x^2 - \log(1 - x^2)$, and the polynomial $(1 - x^2)$ may be considered as a toy fermion determinant. The bosonic action is quadratic and seems to be safe from the blow-up, but now the blow-up arises from the fermion determinant. The gradient flow (4.1) is written as

$$\frac{d}{dt}x(t) = 2x + \frac{2x}{1 - x^2}. \tag{4.7}$$

Here we consider a initial condition $x(0) = x_0$ with $0 < x_0 < 1$. The force term $(\partial S/\partial x)^*$ is real, and x is real for any flow time t. We can solve the differential equation (4.7) analytically, and obtain

$$x(t) = \sqrt{1 - \sqrt{1 - x_0^2(2 - x_0^2)e^{8t}}}. \tag{4.8}$$

The solution reaches the singular point $x = 1$ when $t = (1/8)\log(1/(x_0^2(2 - x_0^2)))$.

More generally, let us consider the fermion determinant $D(z)$ is a multivariable polynomial function written as $D(z) = \prod_i (z - \lambda_i)^{m_i}$. As z approaches the zeros of the fermion determinant, the real part of the action goes to infinity. Thus the points close to the zeros flow into them. We consider a point close to a zero λ that has multiplicity k, and write as $z = \lambda + \delta z$ with $\delta r = \sqrt{\delta z_i^* \delta z_i} \ll 1$. δr behaves as

$$\frac{d}{dt}\delta r \approx -\frac{k}{\delta r}, \tag{4.9}$$

and the solution is given as $\delta r \approx \sqrt{\delta r_0^2 - 2kt}$, where δr_0 is the initial condition.

Now, for the flow time T_{flow} we define a subset of the integration contour $\mathcal{C}_{\mathbb{R}}$ as

$$\mathcal{C}_{\text{fin}} = \{x \in \mathcal{C}_{\mathbb{R}} \mid \|\Phi_{T_{\text{flow}}}(x)\| < \infty\}, \tag{4.10}$$

where $\Phi_{T_{\text{flow}}}$ is the map given by flowing the initial point x up to the flow time T_{flow}. Then, the path integral is written as

$$Z = \int_{\mathcal{C}(T_{\text{flow}})} d^n z \exp(-S(z)) = \int_{\mathcal{C}_{\text{fin}}} d^n x \, \det V(T_{\text{flow}}, x) \exp(-S(\Phi_{T_{\text{flow}}}(x))). \tag{4.11}$$

Here, the flowed contour $\mathcal{C}(T_{\text{flow}})$ is considered as the image of the subset $\mathcal{C}_{\text{fin}}$. For a sufficiently small flow time the subset $\mathcal{C}_{\text{fin}}$ is equivalent to the original integration contour $\mathcal{C}_{\mathbb{R}}$. However as the flow time T_{flow} increases, it may shrinks to the vicinities of the intersection points x_σ, where the original contour $\mathcal{C}_{\text{R}}$ and the dual thimbles $\mathcal{K}_\sigma$ intersect. Then the flowed contour consists of the disconnected regions, which correspond to the union of Lefschetz thimbles contributing to the path integral. The discontinuity is the obstacle to implement the Monte Carlo simulations. We note that the blow-up does not break the equivalence of the complex integral by deforming the integration contour, but is the problem of implementing the numerical simulations.

4.2 Properties of gradient flows without blow-up

In this section, we define a new gradient flow. This flow is similar to the conventional gradient flow, but a positive factor is introduced so that the flow slows down as the action goes to infinity. We show that the blow-up is absent in the new gradient flow.

4.2.1 Formulation

Here we define a new gradient flow as

$$\frac{d}{dt}z_i(t) = g(z, z^*)\left(\frac{\partial S}{\partial z_i}\right)^*, \tag{4.12}$$

where $g(z, z^*)$ is a positive real number. The flow with a positive constant function $g(z, z^*)$ corresponds to the conventional gradient flow (4.1). We specify $g(z, z^*)$ later. Using Eq. (4.12), we have

$$\frac{d}{dt}\mathrm{Re}S = \frac{1}{2}\left(\frac{\partial S}{\partial z_i}\frac{dz_i}{dt} + \left(\frac{\partial S}{\partial z_i}\right)^*\left(\frac{dz_i}{dt}\right)^*\right) = g\left(\frac{\partial S}{\partial z_i}\right)^*\frac{\partial S}{\partial z_i} \geq 0, \tag{4.13}$$

$$\frac{d}{dt}\mathrm{Im}S = \frac{1}{2i}\left(\frac{\partial S}{\partial z_i}\frac{dz_i}{dt} - \left(\frac{\partial S}{\partial z_i}\right)^*\left(\frac{dz_i}{dt}\right)^*\right) = 0. \tag{4.14}$$

Thus as the flow time increases, the real part of the action $\mathrm{Re}S$ increases monotonically, whereas the phase $\exp(-\mathrm{Im}S)$ is constant.

4.2.2 Absence of blow-up

g may be considered as a factor which determines the speed of the flow. When the flow approaches the blow-up regions, g need to be suppressed to balance the force term $g(\partial S/\partial z_i)^*$. One of the example may be given as

$$g = e^{-\mathrm{Re}(S_B(z))/\Lambda_B}\left(\frac{|\det D|^2}{|\det D|^2 + \Lambda_F^{-2}}\right)^\eta, \tag{4.15}$$

where $\Lambda_B, \Lambda_F \geq 1$ are regularization parameters and $\eta \geq 1$ is a parameter which determines the asymptotic behavior in the vicinity of the zeros of the fermion determinant. Here the action is written as $S(z) = S_B(z) - \log\det D(z)$, where the bosonic action $S_B(z)$ and the fermion determinant $\det D(z)$ are polynomial.

We show that the choice (4.15) avoids the blow-up. The blow-up happens when the action diverges and the divergence is classified into the following cases:

$$1.\ \mathrm{Re}(S_B(z)) \to \infty, \tag{4.16}$$

$$2.\ \log D(z) \to 0. \tag{4.17}$$

In the first case, z approaches infinity since S_B is polynomial. In the second case, z approaches a zero of $\log D(z)$. Thus it is sufficient to check these cases.

Here the gradient flow equation (4.12) is written as

$$\frac{d}{dt}z_i(t) = e^{-\mathrm{Re}(S_B(z))/\Lambda_B}\left(\frac{|\det D|^2}{|\det D|^2 + \Lambda_F^{-2}}\right)^\eta\left[\left(\frac{\partial S_B}{\partial z_i}\right)^* - \frac{1}{(\det D)^*}\left(\frac{\partial \det D}{\partial z_i}\right)^*\right]. \tag{4.18}$$

As z approaches infinity, the right-hand side of Eq. (4.18) decreases exponentially. Thus $z(t)$ grows logarithmically at most. As z approaches a zero λ of the fermion determinant $\det D(z)$, the fermion determinant behaves as $\det D(z) \propto (z-\lambda)^k$ with a positive integer k. Thus neglecting subleading terms, we have

$$\frac{d}{dt}|z-\lambda| \approx -c|z-\lambda|^{2\eta k-1}, \tag{4.19}$$

where c is a positive constant. We then obtain $|z-\lambda| \approx \kappa t^{-1/(2\eta k-2)}$ with a positive constant κ when $\eta k > 1$, and $|z-\lambda| \approx \kappa' \exp(-ct)$ with a positive constant κ' when $\eta k = 1$. Therefore in both limits, the flow does not reach the singularities in a finite time.

Chapter 5

HMC on the flowed contour without blow-up

In this chapter we construct the hybrid Monte Carlo algorithm on the the flowed contour using the gradient flow without the blow-up. The flowed contour by the gradient flow without the blow-up is a connected region, and thus the transition between the regions close to different Lefschetz thimbles is possible. We apply the algorithm to the $(0+1)$-dimensional massive Thirring model at finite density, which is a fermionic model with auxiliary fields. We show that the result we obtain agree with the analytic result, as opposed to the conventional generalized Lefschetz thimble method. We also show that the sign problem is mild and the configuration is distributed over the multiple thimbles.

5.1 Construction of the algorithm

In this section, we discuss the hybrid Monte Carlo using the gradient flow without the blow-up,

$$\frac{d}{dt}z_i(t) = g(z, z^*)\left(\frac{\partial S}{\partial z_i}\right)^*, \tag{5.1}$$

where g is a positive function, and we specify it later.

5.1.1 Projection onto tangent space

To solve the molecular dynamics on the flowed contour $\Sigma \coloneqq \mathcal{C}(T_{\text{flow}})$, we need to specify the tangent space $T_z\Sigma$. The flowed contour is derived by solving Eq. (5.1) with the initial condition $z_i(0) = x_i \in \mathcal{C}_{\mathbb{R}}$ up to the flow time T_{flow}. The associated tangent vectors are derived by solving the differential equations,

$$\frac{d}{dt}V_i^\alpha(t) = 2\text{Re}\left(\frac{\partial g}{\partial z_j}V_j^\alpha\right)\left(\frac{\partial S}{\partial z_i}\right)^* + g\left(\frac{\partial^2 S}{\partial z_i \partial z_j}V_j^\alpha\right)^*. \tag{5.2}$$

with the initial condition $V_i^\alpha(0) = \delta_i^\alpha$. We note that the reality condition (2.48) does not hold if g is not a constant function. Thus some modifications are required to implement the hybrid Monte Carlo on the flowed contour. To construct projection operator P_z on the tangent space $T_z\Sigma$, we use the QR decomposition of the tangent vectors V_i^α as

$$\begin{pmatrix} V^{(R)} \\ V^{(I)} \end{pmatrix} = \begin{pmatrix} Q^{(R)} & \tilde{Q}^{(R)} \\ Q^{(I)} & \tilde{Q}^{(I)} \end{pmatrix} \begin{pmatrix} R \\ O \end{pmatrix}. \tag{5.3}$$

$V^{(R)}, V^{(I)}$ are $n \times n$ real matrices satisfying $V_i^\alpha = V_i^{(R)\alpha} + iV_i^{(I)\alpha}$, and $Q^{(R)}, Q^{(I)}, \tilde{Q}^{(R)}, \tilde{Q}^{(I)}$ are $n \times n$ real matrices satisfying

$$Q_i^{(R)\alpha} Q_i^{(R)\beta} + Q_i^{(I)\alpha} Q_i^{(I)\beta} = \delta^{\alpha\beta}, \tag{5.4}$$
$$\tilde{Q}_i^{(R)\alpha} \tilde{Q}_i^{(R)\beta} + \tilde{Q}_i^{(I)\alpha} \tilde{Q}_i^{(I)\beta} = \delta^{\alpha\beta}, \tag{5.5}$$
$$Q_i^{(R)\alpha} \tilde{Q}_i^{(R)\beta} + Q_i^{(I)\alpha} \tilde{Q}_i^{(I)\beta} = 0. \tag{5.6}$$

$R^{\alpha\beta}$ is an $n \times n$ upper triangular matrix with real elements, and the diagonal element is positive [1)]. We note that the inner product of complex vectors $u, v \in \mathbb{C}^n$ is defined by

$$\langle u, v \rangle = \mathrm{Re}(u_i^* v_i), \tag{5.7}$$

and the decomposition gives an orthogonal basis. In the representation using complex vectors, we have

$$V = \begin{pmatrix} Q & \tilde{Q} \end{pmatrix} \begin{pmatrix} R \\ O \end{pmatrix}, \tag{5.8}$$

where $Q_i^\alpha, \tilde{Q}_i^\alpha$ are complex matrices satisfying

$$\mathrm{Re} Q_i^{\alpha *} Q_i^\beta = \delta^{\alpha\beta}, \tag{5.9}$$
$$\mathrm{Re} \tilde{Q}_i^{\alpha *} \tilde{Q}_i^\beta = \delta^{\alpha\beta}, \tag{5.10}$$
$$\mathrm{Re} Q_i^{\alpha *} \tilde{Q}_i^\beta = 0. \tag{5.11}$$

Thus the tangent space $T_z\Sigma$ is spanned by the tangent vectors $\{Q_i^\alpha\}$, and the normal space $N_z\Sigma$ is spanned by the normal vectors $\{\tilde{Q}_i^\alpha\}$. The projection of a complex vector $w_i \in \mathbb{C}^n$ onto the tangent space $T_z\Sigma$ is given by

$$P_z : w_i \mapsto Q_i^\alpha \langle Q^\alpha, w \rangle. \tag{5.12}$$

[1)] Generally, we can decompose an $m \times n$ real matrix M into an $m \times n$ matrix Q with real orthogonal columns and an $n \times n$ upper triangular matrix R with real elements. The factorization is unique if the matrix M is invertible. Here, the differential equation (5.2) is linear over $\mathbb{R}$, since the blow-up does not occur. Then the map of the tangent vectors $V_i^\alpha(0) = \delta_i^\alpha \in T_x\mathcal{C}_\mathbb{R}$ to the flowed tangent vectors $V_i^\alpha(T_{\mathrm{flow}}) \in T_z\Sigma$ is linear, and the tangent vectors $\{V_i^\alpha\}$ are linearly independent over $\mathbb{R}$. Therefore, $Q^{(R)}, Q^{(I)}$ and R are uniquely determined, and $\tilde{Q}^{(R)}, \tilde{Q}^{(I)}$ are determined up to an n-dimensional rotation.

5.1.2 Molecular dynamics

Here, the molecular dynamics on the contour Σ is given by

$$\frac{dz_i}{d\tau} = w_i, \tag{5.13}$$

$$\frac{dw_i}{d\tau} = -\left(\frac{\partial S}{\partial z_i}\right)^* - \tilde{Q}_i^\alpha \lambda^\alpha, \tag{5.14}$$

where $\lambda^\alpha \in \mathbb{R}$ are the Lagrange multipliers.

z_i is constrained on the flowed contour Σ and w_i is constrained on the tangent space $T_z\Sigma$. the conserved Hamiltonian is given by

$$H = \frac{1}{2} w_i^* w_i + \mathrm{Re}[S(z)], \tag{5.15}$$

since

$$\frac{dH}{d\tau} = -\langle w, Q^\alpha \lambda^\alpha \rangle = 0. \tag{5.16}$$

Eqs. (5.13) and (5.14) are discretized as follows:

$$w_i(n+1/2) = w_i(n) - 1/2\Delta\tau \left(\frac{\partial S}{\partial z_i}\right)^*\Big|_{z(n)} - 1/2\Delta\tau \tilde{Q}_i^\alpha(z(n))\lambda_1^\alpha, \tag{5.17}$$

$$z_i(n+1) = z_i(n) + \Delta\tau w_i(n+1/2), \tag{5.18}$$

$$w_i(n+1) = w_i(n+1/2) - 1/2\Delta\tau \left(\frac{\partial S}{\partial z_i}\right)^*\Big|_{z(n+1)} - 1/2\Delta\tau \tilde{Q}_i^\alpha(z(n+1))\lambda_2^\alpha, \tag{5.19}$$

where $\lambda_1^\alpha, \lambda_2^\alpha$ are determined so that $z(n+1) \in \Sigma$ and $w(n+1) \in T_z\Sigma$.

We may use the fixed point iteration method or Newton's method to solve the equations. In these methods we set an initial guess $(z_j^{(0)}, \lambda_{1(0)}^\alpha) = (z_j(n), 0)$, and generate a sequence $(z_j^{(k)}, \lambda_{1(k)}^\alpha)$. Then the solution $(z_j(n+1), \lambda_1^\alpha)$ is obtained by the limit of the sequence, if the step size $\Delta\tau$ is sufficiently small. Here we define

$$\tilde{z}_i \coloneqq z_i(n) + \Delta s w_i(n) - 1/2(\Delta s)^2(\partial_i S(z(n)))^*. \tag{5.20}$$

In the fixed point iteration method, we obtain the solution $z(n+1)$ by solving the recurrence relation,

$$\Delta x_\alpha^{(k+1)} = -R_{\alpha\beta}^{-1}\mathrm{Re}[Q_j^{\beta *}(z_j^{(k)} - \tilde{z}_j)], \tag{5.21}$$

$$x_\alpha^{(k+1)} = x_\alpha^{(k)} + \Delta x_\alpha^{(k+1)}, \tag{5.22}$$

$$z_i^{(k+1)} = \Phi_i[x^{(k+1)}], \tag{5.23}$$

where Φ_i is the map flowing the initial point $x \in \mathcal{C}_{\mathbb{R}}$ to the point $z \in \Sigma$.

In Newton's method, we obtain the solution $(z(n+1), \lambda)$ by solving the recurrence relation,

$$\begin{pmatrix} \Delta x^{(k+1)} \\ \Delta\lambda_{1(k+1)} \end{pmatrix} = \begin{pmatrix} V^{(k)} & \tilde{Q} \end{pmatrix}^{-1} (-z_i^{(k)} + \tilde{z} - \tilde{Q}^{\alpha}\lambda^{\alpha}_{1(k)}), \tag{5.24}$$

$$x^{(k+1)} = x^{(k)} + \Delta x^{(k+1)}, \tag{5.25}$$

$$z^{(k+1)} = \Phi[x^{(k+1)}], \tag{5.26}$$

$$V^{(k+1)} = \Psi[x^{(k+1)}], \tag{5.27}$$

$$\lambda_{1(k)} = \lambda_{1(k)} + \Delta\lambda_{1(k+1)}, \tag{5.28}$$

where Ψ_i^{α} is the map flowing the initial tangent vector δ_i^{α} at $x \in \mathcal{C}_{\mathbb{R}}$ to the tangent vector $V_i^{\alpha} \in T_z\Sigma$.

After obtaining the solution $(z(n+1), \lambda_1^{\alpha})$, we compute the QR decomposition of the tangent vectors $V_i^{\alpha}(z(n+1))$. Since $w_i(n+1)$ is constrained on the tangent space $T_{z(n+1)}\Sigma$, we have

$$w_i(n+1) = Q_i^{\alpha}|_{z(n+1)} \,\mathrm{Re}\left(Q_j^{\alpha *}\big|_{z(n+1)} \left[w_j(n+1/2) - 1/2\Delta\tau \left(\frac{\partial S}{\partial z_j} \right)^* \Big|_{z(n+1)} \right] \right). \tag{5.29}$$

5.1.3 Residual phase

Now we discuss the residual phase. The flowed contour Σ is embedded in $\mathbb{R}^{2n}$ by the map $z \mapsto (\mathrm{Re}z, \mathrm{Im}z)$, as we construct the orthonormal basis of the tangent vectors $\{Q_i^{\alpha}\}$ and normal vectors $\{\tilde{Q}_i^{\alpha}\}$ by the QR decomposition (5.3). The point in the vicinity of z is parametrized by the coordinates $\delta\xi^{\alpha}$ as $\delta z_i = Q_i^{\alpha}\delta\xi^{\alpha}$, and the molecular dynamics is constrained on the real manifold $\mathbb{M} \subset \mathrm{R}^{2n}$, which is parametrized by the local coordinates $\{\xi^{\alpha}\}$. Thus from the measured configurations $z^{(k)}\,(k = 1, \ldots, N_{\mathrm{conf}})$, we estimate the expectation value of an observable $O(z)$ as

$$\frac{1}{Z_0}\int_{\mathbb{M}} d^n\xi\, e^{-\mathrm{Re}S(z(\xi))} O(z(\xi)) \approx \frac{1}{N_{\mathrm{conf}}} \sum_{k=1}^{N_{\mathrm{conf}}} O(z^{(k)}), \tag{5.30}$$

where

$$Z_0 = \int_{\mathbb{M}} d^n\xi\, e^{-\mathrm{Re}S(z(\xi))}. \tag{5.31}$$

Since the complex integral is related to the real integral of the real coordinates ξ^{α} by Eq. (2.21), we need to compensate the Jacobian determinant $\det Q$ and the phase factor $e^{-i\mathrm{Im}S(z)}$ as,

$$\langle O \rangle \approx \frac{N_{\mathrm{conf}}^{-1} \sum_k \det Q(z^{(k)}) e^{-i\mathrm{Im}S(z^{(k)})} O(z^{(k)})}{N_{\mathrm{conf}}^{-1} \sum_k \det Q(z^{(k)}) e^{-i\mathrm{Im}S(z^{(k)})}}. \tag{5.32}$$

By the QR decomposition, Q is uniquely determined, but $\det Q$ is also explicitly represented by the tangent vectors $\{V_i^\alpha\}$ through

$$\det Q = \frac{\det V}{\sqrt{\det(\mathrm{Re}(V^\dagger V))}}. \tag{5.33}$$

To evaluate $\det Q$, we consider the properties of the n-dimensional complex basis $\{Q_i^\alpha\}$. Since Eq. (5.9) include $1/2n(n+1)$ constraints, Q is an element of the $(2n^2 - 1/2n(n+1))$-dimensional compact manifold. We introduce the real matrices Q_R, Q_I as $Q = Q_R + iQ_I$. Then the condition (5.9) is rewritten as

$$Q_R^T Q_R + Q_I^T Q_I = I, \tag{5.34}$$

and the matrix Q is decomposed into the following form:

$$Q = L_1 \mathrm{diag}(\cos\theta_1, \ldots, \cos\theta_n) R + iL_2 \mathrm{diag}(\sin\theta_1, \ldots, \sin\theta_n) R, \tag{5.35}$$

where L_1, L_2, R are the $n \times n$ orthogonal matrix and $0 \le \theta \le \pi/2$. We note that the total number of degrees of freedoms of orthogonal matrices L_1, L_2, R and the parameters θ agree with that of the condition (5.9) as

$$1/2n(n-1) \times 3 + n = 2n^2 - 1/2n(n+1). \tag{5.36}$$

If the reality condition (2.48) is satisfied, we have $\mathrm{Im} Q_i^{\alpha *} Q_i^\beta = 0$ and Q is a unitary matrix. Thus we have

$$Q_R Q_R^T + Q_I Q_I^T = I, \tag{5.37}$$

and the matrix Q is decomposed into the following form:

$$Q = L \mathrm{diag}(e^{i\theta_1}, \ldots, e^{i\theta_n}) R, \tag{5.38}$$

where L, R are the $n \times n$ orthogonal matrices whose determinants are 1, and $0 \le \theta < 2\pi$.

From Eq. (5.35), we can write Q as

$$Q = P_1 H_1 + iP_2 H_2, \tag{5.39}$$

where H_1, H_2 are the commutative Hermitian matrices satisfying $H_1^2 + H_2^2 = 1$ and P_1, P_2 are the orthogonal matrices. Then we have

$$Q^\dagger Q = 1 + i(H_1 P_1^T P_2 H_2 - H_2 P_2^T P_1 H_1) =: 1 + iA, \tag{5.40}$$

where A is the antisymmetric real matrix. By introducing a matrix,

$$B \equiv H_1 P_2^T P_1 H_1 + H_2 P_1^T P_2 H_2, \tag{5.41}$$

we have the equation,

$$(iA)^\dagger(iA) + B^\dagger B = I. \tag{5.42}$$

Thus the eigenvalues $\lambda_i(iA)\,(i = 1, \ldots, n)$ of the Hermitian matrix iA are bounded by $-1 \leq \lambda_i(iA) \leq 1$.

From this bound, the eigenvalues of the matrix Q are bounded by

$$|\lambda_i(Q)| \leq \sqrt{\max \lambda_i(Q^\dagger Q)} = \sqrt{2}. \tag{5.43}$$

For example, 2×2 matrix,

$$\begin{pmatrix} \cos(\pi/4) & -i\sin(\pi/4) \\ i\sin(\pi/4) & \cos(\pi/4) \end{pmatrix} \tag{5.44}$$

has the eigenvalues $0, \sqrt{2}$, and the equality of (5.43) holds. Since A is the antisymmetric matrix, the eigenvalues come in pairs $\pm\lambda_i\,(i = 1, \ldots, n')$ except for the zero eigenvalues, and we have

$$\det(Q^\dagger Q) = \prod_{i=1}^{n'}(1 - \lambda_i^2) \leq 1. \tag{5.45}$$

Therefore we have $|\det Q| \leq 1$. The equality $|\det Q| = 1$ holds, if and only if the flowed tangent vectors $V_i^\alpha \in T_z\Sigma$ satisfy the reality condition (2.48), which is derived in the conventional gradient flow. If $|\det Q| \ll 1$, the evaluation (5.32) is not valid numerically and we suffer from the sign problem. However we expect that $|\det Q|$ is close to unity, since as the flow time increases the flowed contour approaches the Lefschetz thimbles, on which the reality condition is satisfied.

5.1.4 Summary of the algorithm

Here we briefly summarize the hybrid Monte Carlo update on the flowed contour Σ.

1. Set the initial configuration x_i and compute

$$z_i = \Phi_i(x), \quad V_i^\alpha = \Psi_i^\alpha(x) \tag{5.46}$$

by the Runge-Kutta method. Also compute the QR decomposition (5.8) of the tangent vectors V_i^α. Here $\Phi_i(x)$ is the solution of Eq. (5.1) at the flow time T_{flow} with the initial condition $z_i(0) = x_i$. Similarly, $\Psi_i^\alpha(x)$ is the solution of Eq. (5.2) at the flow time T_{flow} with the initial condition $V_i^\alpha(0) = \delta_i^\alpha$.

2. Generate n pairs of unit Gaussian random numbers $\xi_i, \eta_i\,(i = 1, \ldots, n)$. Then the tentative momenta $w_i = \xi_i + i\eta_i$ are projected on the tangent space $T_z\Sigma$ by

$$w_i = Q_i^\alpha \mathrm{Re}(Q_j^{\alpha *} w_j). \tag{5.47}$$

3. Iteratively compute the discretized molecular dynamics (5.17)-(5.19) using the fixed point iteration method or Newton's method. In Eqs. (5.17)-(5.19), we update $z_i = \Phi_i(x)$, $V_i^\alpha = \Psi_i^\alpha(x)$ and the QR decomposition.

4. Accept the proposed configuration (w', z') by the probability $\min\{1, e^{-\Delta H}\}$, where $\Delta H = H(w', z') - H(w, z)$.

5. After repeating step 2 to step 4 sufficiently many times , get a configuration z and compute the determinant $\det Q$.

6. After repeating step 2 to step 5, obtain a sequence of the configurations $z^{(1)}, \ldots, z^{(N_{\rm conf})}$ and evaluate the expectation value of an observable $O(z)$ by Eq. (5.32).

5.1.5 Computational cost

The difference between the flow without the blow-up and the conventional flow arises in the computation of g in Eqs. (5.1) and (5.2), and the QR decomposition of the tangent vectors $\{V_i^\alpha\}$. For example, the fermion determinant $\det D$ appears in Eq. (4.15), and requires the computation scaling as $\mathcal{O}(n^3)$ iteratively in the Runge-Kutta method. It is the dominant part of the computation in fermionic models, and we need an improvement of the choice of g. The computation of QR decomposition scales as $\mathcal{O}(n^3)$, whereas that of inverse matrix V^{-1} used to project complex vectors on the tangent space in the conventional flow scales as $\mathcal{O}(n^2)$ by the iterative method, for example, the conjugate gradient method.

5.2 Massive Thirring model at finite density

We examine the hybrid Monte Carlo algorithm on the flowed contour Σ without the blow-up by applying it to the $(0+1)$-dimensional massive Thirring model at finite density [13, 14, 40, 41, 44–48].

5.2.1 Model

We start from the d-dimensional massive Thirring model. The path integral in the continuum is given by

$$Z = \int d\psi d\bar{\psi} e^{-\int d^d x \, \mathcal{L}(\psi, \bar{\psi})}, \tag{5.48}$$

where the action is

$$\mathcal{L}(\psi, \bar{\psi}) = \sum_f \bar{\psi}^f (\partial_\mu \gamma^\mu + m_f + \mu_f \gamma^0) \psi^f + \frac{g^2}{2N_F} \left(\bar{\psi}^f \gamma_\mu \psi^f\right) \left(\bar{\psi}^{f'} \gamma^\mu \psi^{f'}\right). \tag{5.49}$$

Here the index $f, f' = 1, \ldots, N_F$ denotes the fermion flavors. The γ matrices satisfy the anticommutation relation $\gamma_\mu, \gamma_\nu = 2\delta_{\mu\nu}$. For example, γ matrices for $d = 2$ are given by

$$\gamma^0 = \begin{pmatrix} 0 & 1 \\ 1 & 0 \end{pmatrix}, \quad \gamma^1 = \begin{pmatrix} 0 & -i \\ i & 0 \end{pmatrix}. \tag{5.50}$$

We impose the following boundary condition:

$$\psi(x + \beta\hat{0}) = -\psi(x), \tag{5.51}$$

$$\psi(x + L\hat{i}) = \psi(x), \quad i = 1, \ldots, d-1, \tag{5.52}$$

where $\hat{i}$ denote the unit vectors in the direction x_i. Introducing auxiliary fields $A_\mu(x)$, we can write the path integral as

$$Z = \int dA \int d\psi d\bar{\psi} e^{-\int d^d x \, \mathcal{L}(A,\psi,\bar{\psi})}, \tag{5.53}$$

where

$$\mathcal{L}(A, \psi, \bar{\psi}) = \sum_f \bar{\psi}^f (\gamma^\nu(\partial_\nu + iA_\nu) + m_f + \mu_f \gamma^0)\psi^f + \frac{N_F}{2g^2} A_\nu A^\nu. \tag{5.54}$$

After integrating out the fermion fields, we obtain

$$Z = \int dA \, e^{-S_A} \prod_f \det D_f(A, \mu), \tag{5.55}$$

where

$$S_A = \frac{N_F}{2g^2} \int d^d x \, A_\nu A^\nu. \tag{5.56}$$

Here we introduce an operator $D_f = \gamma^\mu(\partial_\mu + iA_\mu) + m_f + \mu_f\gamma^0$. We note that the fermion determinant satisfies the relation,

$$\det D_f(A, \mu_f)^* = \det D_f(A, -\mu_f^*). \tag{5.57}$$

Thus for $\mu_f > 0$ the path integral is complex, and suffers from the sign problem.

5.2.2 Discretization

Now we discretize the action. On the lattice, the chemical potential is introduced like the zero-th component of an imaginary constant gauge field, according to the prescription by Ref. [49]. The fermion field are defined on the lattice by the Wilson fermions [50] or the staggered fermions [51, 52]. Then the lattice action for Wilson fermions is given by

$$S_{\text{lat}}(A, \psi, \bar{\psi}) = \sum_{x,\nu} \frac{N_F}{g^2}(1 - \cos a A_\nu(x)) + \sum_{f,x,y} \bar{\psi}^f(x) \left(D^W\right)^f_{xy} \psi^f(y), \tag{5.58}$$

where the operator D^W is given by

$$\left(D^W\right)^f_{xy} = \delta_{x,y} - \kappa_f \sum_\nu \left[(1-\gamma_\nu)e^{iA_\nu(x)+\mu_f\delta_{0,\nu}}\delta_{x+\nu,y} + (1+\gamma_\nu)e^{-iA_\nu(x)-\mu_f\delta_{0,\nu}}\delta_{x,y+\nu}\right], \tag{5.59}$$

with $1/\kappa_f = 2m_f + 2d$. The lattice action for staggered fermions is given by

$$S_{\rm lat}(A,\chi,\bar\chi) = \sum_{x,\nu}\frac{N_F}{g^2}(1-\cos A_\nu(x)) + \sum_{f,x,y}\bar\chi^f(x)\left(D^{KS}\right)^f_{xy}\chi^f(y), \tag{5.60}$$

where χ^f and $\bar\chi^f$ denote staggered fermion fields with no spinor indices. The flavor index runs $f = 1,\ldots,N_F/2^{\lfloor d/2\rfloor}$, since the fermion doubling accounts for the flavors [2)]. The operator D^{KS} is given by

$$\left(D^{KS}\right)^f_{xy} = m_f\delta_{x,y} + \frac{1}{2}\sum_\nu \eta_\nu(x)\left[e^{iA_\nu(x)+\mu_f\delta_{0,\nu}}\delta_{x+\nu,y} - e^{-iA_\nu(x)-\mu_f\delta_{0,\nu}}\delta_{x,y+\nu}\right], \tag{5.61}$$

with the phase factor $\eta_\nu(x) = (-1)^{x_0+\cdots+x_{\nu-1}}$. Here, we adopt the staggered lattice action. After integrating out the fermion fields, we thus obtain

$$Z = \int_{-\pi}^{\pi}\left(\prod_{x,\nu}\frac{dA_\nu(x)}{2\pi}\right)e^{-1/g^2\sum(1-\cos A_\nu(x))}\left(\prod_a \det D^{KS}_a\right). \tag{5.62}$$

In (0+1)-dimensional massive Thirring model, we can solve the integral (5.62) explicitly. Here after we consider $N_F = 1$ particularly. Then the path integral we are interested in is given by

$$Z = \int_{-\pi}^{\pi}\left(\prod_{k=1}^{N_t}\frac{dz_k}{2\pi}\right)e^{-\alpha\sum_{k=1}^{N_t}(1-\cos z_k)}\det D(z). \tag{5.63}$$

Here we recover the lattice spacing a, and discretize the Euclidean time by an even number of lattice points N_t as $\beta = N_t a$. Also we introduce a parameter $\alpha = 1/(g^2 a)$. The functional determinant $\det D(z)$ of D is given by

$$\det D(z) = \frac{1}{2^{N_t-1}}\left[\cosh\left(N_t\hat\mu + i\sum_{k=1}^{N_t}z_k\right) + \cosh(N_t\hat m)\right], \tag{5.64}$$

[2)] The fermion doubling is a problem that lattice fermion fields satisfying some fundamental properties describes multiple fermionic particles, which are physically unfavored. The Nielsen-Ninomiya theorem [53,54] states that lattice fermions satisfying translation invariance, chiral symmetry, Hermiticity, quadraticity in the fields, and local inevitably possess the doubling. To solve this problem, we need to break the chiral symmetry explicitly like the Wilson fermions, or regard the doublers as spinors and flavors like the staggered fermions.

where $\hat{\mu} = \mu a$ and $\hat{m} = \sinh^{-1} ma$. We can perform the path integral analytically, and the explicit expression of the integral is given by

$$Z = \frac{1}{2^{N_t-1}} e^{-N_t\alpha} \left[I_1(\alpha)^{N_t} \cosh(N_t\hat{\mu}) + I_0(\alpha)^{N_t} \cosh(N_t\hat{m}) \right], \tag{5.65}$$

where $I_n(x)$ are the modified Bessel functions. From (5.65), we obtain the number density and the fermion condensate as

$$\langle n \rangle \coloneqq \frac{1}{N_t a} \frac{\partial \log Z}{\partial \mu} = \frac{I_1(\alpha)^{N_t} \sinh(N_t\hat{\mu})}{I_1(\alpha)^{N_t} \cosh(N_t\hat{\mu}) + I_0(\alpha)^{N_t} \cosh(N_t\hat{m})}, \tag{5.66}$$

$$\langle \bar{\chi}\chi \rangle \coloneqq \frac{1}{N_t a} \frac{\partial \log Z}{\partial m} = \frac{1}{\cosh(\hat{m})} \frac{I_0(\alpha)^{N_t} \sinh(N_t\hat{m})}{I_1(\alpha)^{N_t} \cosh(N_t\hat{\mu}) + I_0(\alpha)^{N_t} \cosh(N_t\hat{m})}. \tag{5.67}$$

As the lattice spacing a goes to zero, the partition function (5.65) behaves as

$$Z \to \frac{1}{2^{N_t-1}} \left(e^{-\frac{3}{8}\beta g^2} \cosh \beta\mu + e^{\frac{1}{8}\beta g^2} \cosh \beta m \right). \tag{5.68}$$

To derive the asymptotic form (5.68), we used the approximation,

$$I_0(\alpha) \approx \frac{e^\alpha}{\sqrt{2\pi\alpha}} \left(1 + \frac{1}{8}\frac{1}{\alpha} \right), \tag{5.69}$$

$$I_1(\alpha) \approx \frac{e^\alpha}{\sqrt{2\pi\alpha}} \left(1 - \frac{3}{8}\frac{1}{\alpha} \right). \tag{5.70}$$

In the low temperature limit $\beta \to \infty$, the number density and the fermion condensate behave as

$$\langle n \rangle \to H(\mu - \mu_c), \tag{5.71}$$

$$\langle \bar{\chi}\chi \rangle \to 1 - H(\mu - \mu_c), \tag{5.72}$$

where $H(x)$ is the Heaviside step function, and $\mu_c = m + g^2/2$. Therefore the model shows a first-order transition at the critical chemical potential μ_c.

5.2.3 Thirring model in the uniform-field subspace

Before simulating the (0 + 1)-dimensional massive Thirring model, we simulate the Thirring model in the uniform-field subspace, where the thimble structure is explicitly visible. The partition function of this simplified model is given by

$$Z = \int_{-\pi}^{\pi} \frac{dz}{2\pi} e^{-\alpha L(1-\cos z)} \det D(z). \tag{5.73}$$

Here the functional determinant $\det D(z)$ is given by

$$\det D(z) = \frac{1}{2^{L-1}} \left[\cosh(L(\hat{\mu} + iz)) + \cosh(L\hat{m})\right]. \tag{5.74}$$

The path integral is derived by restricting the configuration to the uniform-field subspace $z_i = z\,(i = 1, \ldots, N_t)$ and replacing the number of degrees of freedoms N_t by a parameter L. The partition function is explicitly given by

$$Z = \frac{1}{2^{L-1}} e^{-L\alpha} \left[I_L(L\alpha)\cosh(L\hat{\mu}) + I_0(L\alpha)\cosh(L\hat{m})\right]. \tag{5.75}$$

Thus we obtain the number density and the fermion condensate as

$$\langle n \rangle = \frac{I_L(L\alpha)\sinh(L\hat{\mu})}{I_L(L\alpha)\cosh(L\hat{\mu}) + I_0(L\alpha)\cosh(L\hat{m})}, \tag{5.76}$$

$$\langle \bar{\chi}\chi \rangle = \frac{1}{\cosh(\hat{m})} \frac{I_0(L\alpha)\sinh(L\hat{m})}{I_L(L\alpha)\cosh(L\hat{\mu}) + I_0(L\alpha)\cosh(L\hat{m})}. \tag{5.77}$$

5.3 Test of HMC without blow-up

Now we apply the hybrid Monte Carlo algorithm without the blow-up to the $(0+1)$-dimensional massive Thirring model at finite density, and discuss the result.

5.3.1 Flow factor

To implement the hybrid Monte Carlo algorithm without the blow-up, we need to chose the flow factor g appearing in the gradient flow equations (5.1) and (5.2). As discussed in chapter 4, one of the example is given by

$$g = e^{-\mathrm{Re}(S_B(z))/\Lambda_B} \left(\frac{|\det D|^2}{|\det D|^2 + \Lambda_F^{-2}}\right)^{\eta}. \tag{5.78}$$

There are two cases when the blow-up happens: the divergence coming from the bosonic action and the fermion determinant. In the first case, the flowed point z goes to infinity, but the growth of $z(t)$ is logarithmically slow. In the second case, the flowed point z goes to zeros of the fermion determinant. The behavior in the vicinity of the zero z_0 that the flowed point z approaches depends on the multiplicity k of the zero. When $\eta k > 1$, the flowed point approaches the zero as a power $|z - z_0| \propto t^{-1/(2\eta k - 2)}$. Whereas, when $\eta k = 1$, the flowed point approaches the zero exponentially as $|z - z_0| \propto \exp(-ct)$ with a positive constant c. Fig. 5.1 shows the behavior of the fermion determinant as a function of the flow time for the Thirring model in the uniform-field subspace. In this model, the initial condition $x = 0.1$ flows into a zero of the fermion determinant for

$\alpha = 1, ma = 1, \mu a = 1.5$. When $\eta = 1$, the fermion determinant decrease exponentially. To compute the flow equation (5.1), we use the Runge-Kutta Fehlberg method. In this method the step size is adaptively determined to achieve the required precision. Here we require the estimated error is smaller than 10^{-10}. However the fermion determinant $\det D$ falls below the precision of the computation in a short time if the regularization parameter Λ_F is not suppressed. For the larger flow time, we thus cannot compute the action and its derivatives. If we strongly suppress the regularization parameter Λ_F, the flow factor g is also strongly suppressed and the integration contour is not sufficiently deformed so that the phase fluctuation is mild. The flow with $\eta = 1$ requires the careful adjustment of the flow time and the regularization parameter Λ_F so that the sign problem is mild but the flow does not approaches zeros. However such an adjustment is not practical for all the initial condition x on the real axis. Therefore we use the flow factor (5.78) with $\eta = 2$ in the simulation.

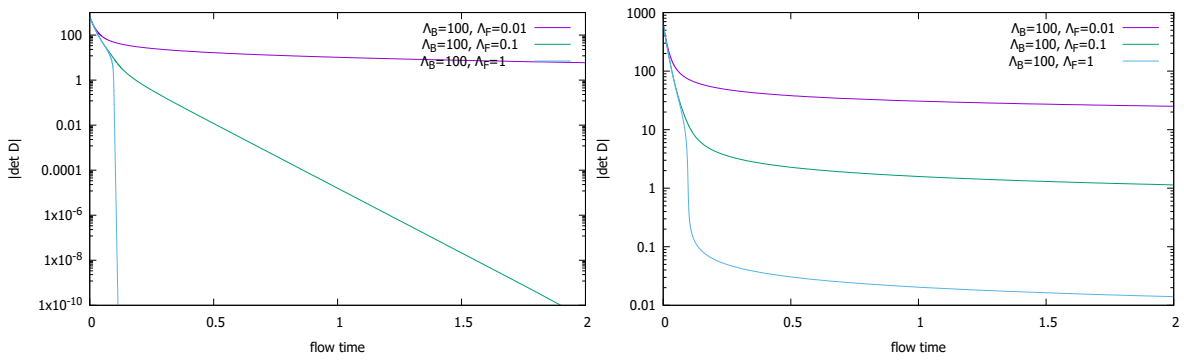

Figure 5.1: Behavior of $|\det D|$ as a function of the flow time. (Left) $\eta = 1$. (Right) $\eta = 2$. Here the other parameters are $L = 8, \alpha = 1, ma = 1, \mu a = 1.5$ and the initial condition $x = 0.1$.

5.3.2 HMC simulation in uniform-field model

Fig. 5.2 shows the flowed contour using the gradient flow without the blow-up (5.1). In the Thirring model in the uniform-field subspace, Lefschetz thimbles are attached to the zeros of the fermion determinant. Thus the contour deformed by the conventional gradient flow (4.1) approaches the zeros and flows into them in a short time. However the contour deformed by the gradient flow without the blow-up (5.1) circumvents the infinity and the zeros of the fermion determinant. Therefore it is a connected region, and we expect the hybrid Monte Carlo simulation on it includes the contribution from the multiple thimbles.

Now, following the steps in Sec. 5.1.4, we apply the hybrid Monte Carlo algorithm to the Thirring model in the uniform-field subspace. In step 1, we set the initial configuration

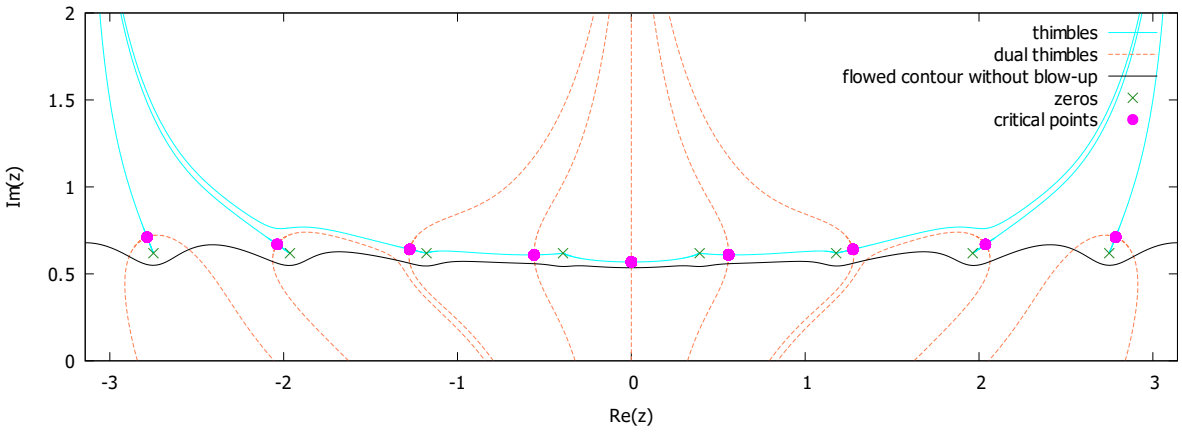

Figure 5.2: Thimbles (solid cyan lines), dual thimbles (dashed coral lines), critical points (magenta blobs), zeros (green crosses), and a flowed contour without blow-up (solid black line) are shown for $L = 8, \alpha = 1, ma = 1, \mu a = 1.5$ and the flow time $T_{\rm flow} = 0.2$.

to the $x = 0$, which flows toward the critical point of the main thimble. We use the Runge-Kutta Fehlberg method to compute Eqs. (5.46). Here we fix the flow time to $T_{\rm flow} = 0.2$. In step 3, we set the step size to $\Delta\tau = 0.02$ and the number of steps to $n_{\rm steps} = 25$. Thus the trajectory length is $\tau_{\rm traj} = 0.5$ for each of the hybrid Monte Carlo update. To compute the discretized molecular dynamics (5.17)-(5.19), we use Newton's method so that the recurrence relation converges more safely. For the thermalization, we discard first 200 configurations generated in step 2 to step 4. We then repeat step 2 to step 4 ten times, and sample the configurations as step 5. In step 6, we estimate the expectation value (5.32) using 1000 configurations out of 10200.

Fig. 5.3 shows the average of $\det Qe^{-i{\rm Im}S}$, which is the denominator in Eq. (5.32). The result is shown for $L = 8, \alpha = 1, ma = 1$. The action is real for the chemical potential $\mu = 0$, and as μ increases the phase $\exp(-i{\rm Im}S)$ fluctuate along the real axis. The blue points represents the result for the original integration contour. It corresponds to the reweighting procedure (2.9), since Q is an identity matrix for the flow time $T_{\rm flow} = 0$. The phase average decreases to nearly zero as the chemical potential μ exceed 1, and the sign problem appears. The green points represents the result for the contour deformed by the conventional gradient flow with $T_{\rm flow} = 0.2$. The average of $\det Qe^{-i{\rm Im}S}$ is near to 1 and the sign problem disappears. The red points represents the contour deformed by the gradient flow without the blow-up with $T_{\rm flow} = 0.2$. The average of $\det Qe^{-i{\rm Im}S}$ is smaller than the contour deformed by the conventional gradient flow for $\mu \gtrsim 1$, but still sufficiently large so that the sign problem is mild. Thus at this point, both the conventional flow and the flow without the blow-up seem to be useful to avoid the sign problem.

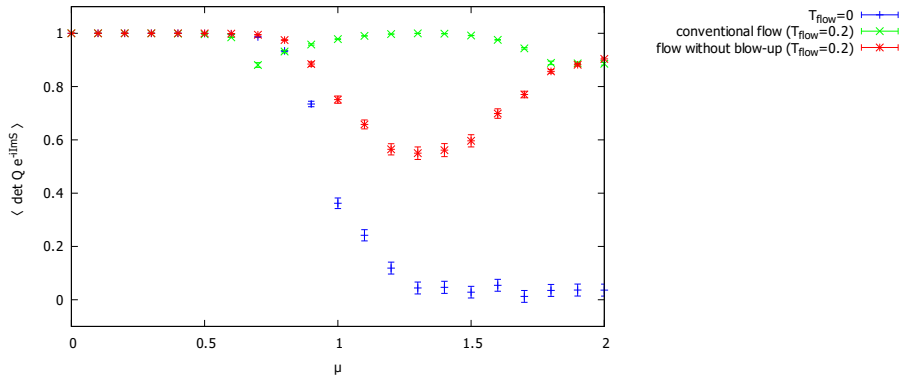

Figure 5.3: Average of $\det Qe^{-i\mathrm{Im}S}$ as a function of the chemical potential μ for the original integration contour (blue), the contour deformed by the conventional gradient flow with $T_{\text{flow}} = 0.2$ (green), and the contour deformed by the gradient flow without the blow-up with $T_{\text{flow}} = 0.2$ (red). The other parameters are $L = 8, \alpha = 1, ma = 1$.

However, a significant difference between the conventional flow and the flow without the blow-up is seen in the evaluation of the expectation value. Fig. 5.4 shows the number density as a function of the chemical potential μ. The solid black line indicates the exact value given by Eqs. (5.76) and (5.77). The green points represents the result for the contour deformed by the conventional gradient flow with $T_{\text{flow}} = 0.2$. They show a small statistical error, but we see a discrepancy between the estimated value and the exact value. The contour deformed by the conventional flow is flowed into the zeros of the fermion determinant, and is separated by those points. In the hybrid Mote Carlo simulation, we start from the configuration $x = 0$. The sequence of the configurations is trapped to the main thimble lying on the center of Fig. 5.2. Thus the result includes the contribution only from the main thimble, and the discrepancy is explained by the contribution from the other subdominant thimbles. The red points represents the result for the contour deformed by the flow without the blow-up with $T_{\text{flow}} = 0.2$. They agree with the exact value, and imply that the estimated value includes the contribution from the multiple thimbles since the flowed contour is a connected region. Thus the difference of the relative phases $e^{-i\mathrm{Im}S(z_\sigma)}$ between the thimbles $\mathcal{J}_\sigma$ decrease the average of $\det Qe^{-i\mathrm{Im}S}$ as seen in Fig. 5.3.

5.3.3 HMC simulation in Thirring model

Now we apply the hybrid Monte Carlo algorithm without the blow-up to the $(0 + 1)$-dimensional massive Thirring model at finite density, where the path integral is given by the multi-dimensional integral. We again follow the steps in Sec. 5.1.4. We fix the

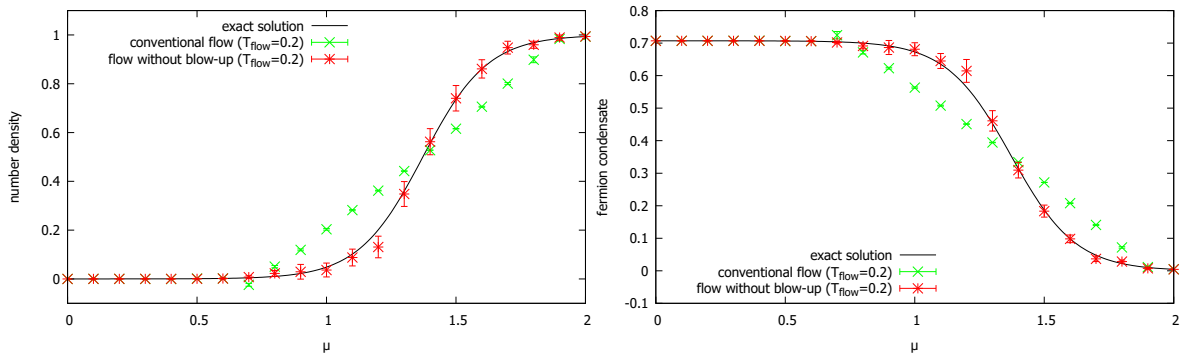

Figure 5.4: Number density and fermion condensate as a function of the chemical potential μ for the conventional flow with $T_{\rm flow} = 0.2$ (green) and the flow without the blow-up with $T_{\rm flow} = 0.2$ (red). The solid black line indicates the exact value. The other parameters are $L = 8, \alpha = 1, ma = 1$.

flow time to $T_{\rm flow} = 1, 2, 3, 4$ and obtain the results with $N_t = 8, \alpha = 1, ma = 1$. We note that the flow time $T_{\rm flow}$ we consider here is much longer than in the uniform-field model, since in the uniformed-field model the force term $g(\partial S/\partial z_i)^*$ in Eq. (5.1) is N_t times larger than in the Thirring model with $z_i = z\,(i = 1, \ldots, N_t)$. Fig. 5.5 shows the average of $\det Q e^{-i{\rm Im}S}$. The average of $\det Q e^{-i{\rm Im}S}$ with the flow time $T_{\rm flow} = 1$ is smaller than that with $T_{\rm flow} \geq 2$, since the flowed contour with $T_{\rm flow} = 1$ is still distant from the Lefschetz thimbles and the fluctuation of the phase $e^{-i{\rm Im}S}$ still remains. For the flow time $T_{\rm flow} \geq 2$, the difference of the average of $\det Q e^{-i{\rm Im}S}$ is small. Thus we expect that the flowed contour with $T_{\rm flow} \geq 2$ sufficiently approaches the Lefschetz thimbles, and the flow time $T_{\rm flow} = 2$ is enough to solve the sign problem.

In the gradient flow without the blow-up, we have $|\det Q| \leq 1$ for multi-dimensional integrals, since the reality condition (2.48) is not satisfied. Thus the smallness of $|\det Q|$ may possibly worsen the sign problem. Fig. 5.6 shows the average of $|\det Q|$ with the flow time $T_{\rm flow} = 2$. The average of $|\det Q|$ is close to 1, and the decrease of the average of $\det Q e^{-i{\rm Im}S}$ in Fig. 5.5 is explained by the fluctuation of the phase of the Jacobian determinant $\det Q$ and the difference of the relative phases $e^{-i{\rm Im}S(z_\sigma)}$ between the thimbles $\mathcal{J}_\sigma$.

Fig. 5.7 shows the number density as a function of the chemical potential μ. The solid black line indicates the exact value given by Eqs. (5.66) and (5.67). The red points represents the result on the contour deformed by the gradient flow without the blow-up with $T_{\rm flow} = 2$. They agree with the exact value, and imply that the estimated value includes the contribution from the multiple thimbles. This is confirmed by Fig. 5.8. In Fig. 5.8 the distribution of $z_{\rm ave} = N_t^{-1} \sum_i z_i$ is shown on a complex plane. The the configurations are distributed across the zero of the fermion determinant, and thus spread over the multiple thimbles.

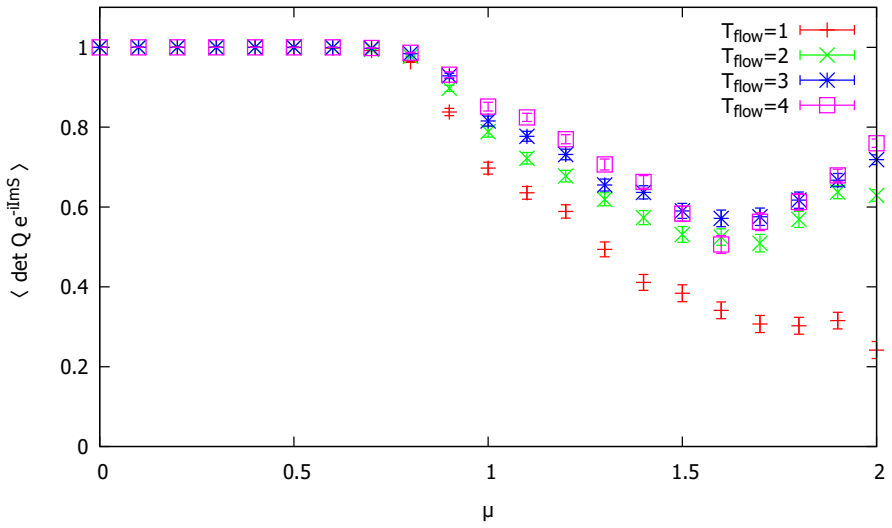

Figure 5.5: Average of $\det Qe^{-i\mathrm{Im}S}$ as a function of the chemical potential μ with the flow time $T_{\mathrm{flow}} = 1, 2, 3, 4$. The other parameters are $N_t = 8, \alpha = 1, ma = 1$.

5.4 Discussion

We point out that in the hybrid Monte Carlo update on the curved space we may possibly fail to compute a proposal. This happens in the step of solving the discretized molecular dynamics (5.17)-(5.19) using the iterative method such as the fixed point iteration method or Newton's method. In some cases, we cannot find a solution by the iterative method, and it is caused by the following two problems.

The first problem comes from the parametrization of a flowed point z. By the gradient flow, a point $x \in \mathcal{C}_{\mathbb{R}}$ in the vicinity of the intersection point of the original integration contour $\mathcal{C}_{\mathbb{R}}$ and a dual thimble $\mathcal{K}_\sigma$ approaches the critical point, and then deviates from it along the thimble $\mathcal{J}_\sigma$. Thus a small region in the vicinity of the intersection point approaches the critical point and then covers the thimble $\mathcal{J}_\sigma$. On the other hand, a point far from the intersection points approaches infinity or zeros of the fermion determinant. Now we consider a contour consisting of a region approaching a thimble and a region approaching a zero. Since the tangent vectors V_i^α is given by the derivative of a flowed point z with respect to an initial condition x as $V_i^\alpha = \partial z_i / \partial x^\alpha$, the norms of the tangent vectors are large in the region approaching a thimble and small in the region approaching a zero. As the flow time increase, the difference of the norms of the tangent vectors between those regions becomes significant. Thus when a point on the region approaching a thimble is shifted toward the region approaching a zero by the hybrid Monte Carlo update, the tangent vectors abruptly change. Then the iterative method may not converge since the sequence of approximate solutions is generated only by the local function with respect

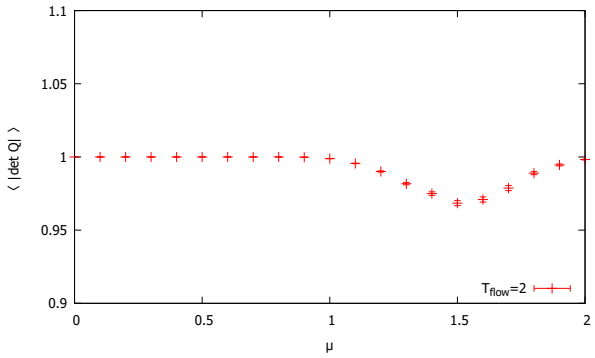

Figure 5.6: Average of $|\det Q|$ as a function of the chemical potential μ with the flow time $T_{\text{flow}} = 2$. The other parameters are $N_t = 8, \alpha = 1, ma = 1$.

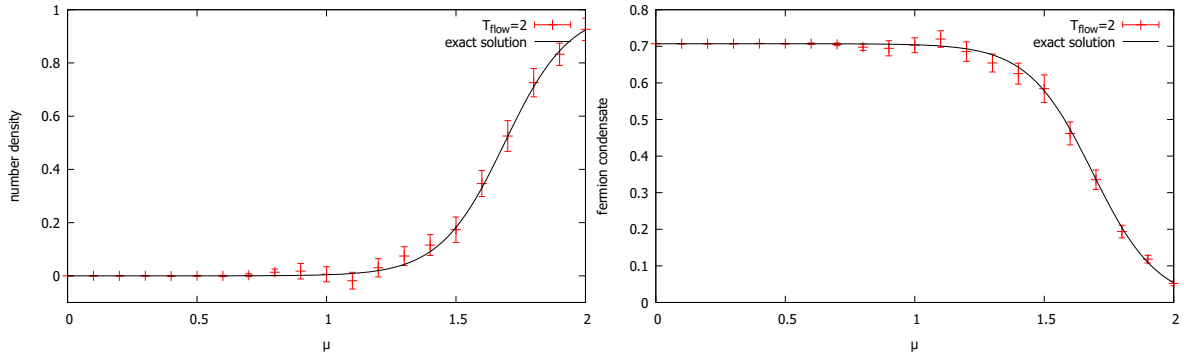

Figure 5.7: Number density and fermion condensate as a function of the chemical potential μ for the flow without the blow-up with $T_{\text{flow}} = 2$ (red). The solid black line indicates the exact value. The other parameters are $N_t = 8, \alpha = 1, ma = 1$.

to the point x on the original integration contour. We note that not the tangent space $T_z\Sigma$ but the basis of the tangent vectors $\{V_i^\alpha\}$ may cause the problem. Thus it can be solved by improving the iterative method. For example, if the $(k+1)$-th approximation $x^{(k+1)} = x^{(k)} + \Delta x$ is worse than $x^{(k)}$ as $|x^{(k+1)} - x_{\text{sol}}| > |x^{(k)} - x_{\text{sol}}|$ with the solution x_{sol}, we may employ $x^{(k+2)} = x^{(k)} + \Delta x/2$ as $(k+2)$-th approximation. This improvement works well if a local minimum does not exist around the solution.

The second problem comes from the shape of the flowed contour. For example, in the vicinity of zeros of the fermion determinant, the directions of the tangent vectors may abruptly change since the zeros connect the thimbles. This problem is more serious because we confront the following three problems. First, if the flowed contour is sharply curved, the solution may not exist. Second, even if we find the solution, the map $(w(n), z(n)) \to (w(n+1), z(n+1))$ by the discretized molecular dynamics (5.17)-(5.19) may not be continuous. Then the Hamiltonian (5.15) jumps and the acceptance rate

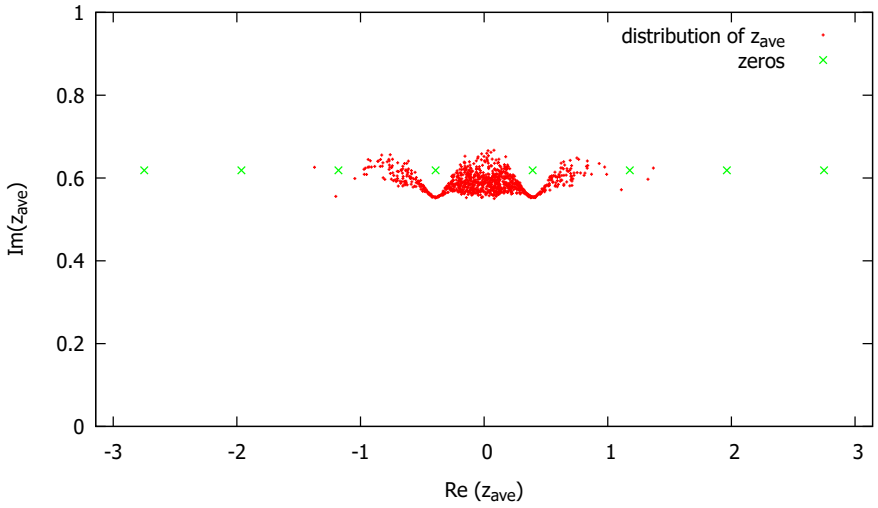

Figure 5.8: Distribution of $z_{\rm ave} = N_t^{-1} \sum_i z_i$ is shown for $L = 8, \alpha = 1, ma = 1, \mu a = 1.5$ on a complex plane (red). Zeros of the fermion determinant $\det D(z)$ is also shown (green).

decreases. Third, the solution may not be unique, and the reversibility (2.51) is not ensured. Thus the detailed balance condition is not satisfied. To avoid these problems we need to adjust the step size $\Delta\tau$ in the discretized molecular dynamics (5.17)-(5.19). We note that the detailed balance condition is slightly broken for an arbitrarily small step size, since the momentum can be arbitrarily large according to the Gaussian distribution. In order to have the detailed balance condition and continue the simulation even if the solution of (5.17)-(5.19) is not found, we take into account the momentum flip as implemented in the parallel-tempering algorithm [14, 15]. However, without the parallel-tempering algorithm, the ergodicity is not assured. Thus we carefully adjusted the step size in the simulation so that we can find a solution.

As an alternative method, we may implement the Metropolis algorithm using the gradient flow without the blow-up. Using a uniform distribution function with a sufficiently small radius r, we have the detailed balance condition (See Appendix). However, we observe a long autocorrelation time, and thus the algorithm is inefficient. For a future study, we leave the improvement of the algorithm using the gradient flow without the blow-up.

We also point out that the computational cost using the flow without the blow-up is more expensive than the conventional flow. It requires the additional computation of g in Eqs. (5.1) and (5.2), and the QR decomposition of the tangent vectors $\{V_i^\alpha\}$. Since the computation of $\det D$ in g, which iteratively appears in the Runge-Kutta method is

$\mathcal{O}(n^3)$, we need to improve the choice of g [3]. One of the alternative choice may be given by using the inverse of the norm of $\partial S_F/\partial z_i$ where $S_F = \log\det D$ instead of $\det D$. Since $\partial S_F/\partial z_i$ and its derivative are also computed in the conventional flow, the computational cost of the gradient flow with the alternative g scales as with the conventional flow. For a future study, we leave the investigation of the algorithm using the gradient flow with the alternative g.

[3] In the $(0+1)$-dimensional massive Thirring model at finite density, the fermion determinant $\det D$ is analytically given by Eq. (5.64). Thus when we use Newton's method to solve the discretized molecular dynamics, the computational cost is similar to that with the conventional flow.

Chapter 6

Summary and Outlook

The sign problem arises from the difficulty of the numerical simulation of the path integral with a complex action, where the integrand gives both the positive and negative contributions and they almost cancel each other out. Thus a huge number of configurations are required to evaluate the integral. This problem appears in many physically interesting systems, for example finite-density QCD and real-time dynamics, and thus it is important to develop the simulation methods which solve this problem.

In Chapter 2, we give a brief review on the Lefschetz thimble method. This method was proposed to solve the sign problem. The point of the Lefschetz thimble method is the complexification of the integration variables and deformation of the integration contour in the complexified space, thanks to Cauchy's integral theorem. To solve the sign problem, we need to find a contour on which the phase fluctuation disappears. Such a contour is formulated by the gradient flow, which is defined by the differential equation with respect to the complexified variables. One of the important property in the gradient flow is that along the flow the real part of the action monotonically increases whereas the imaginary part of the action is constant. Using the gradient flow we can define the contours on which the imaginary part of the action is constant. These contours are called Lefschetz thimbles. The original integration contour is deformed to the linear combination of the Lefschetz thimbles. Therefore, if a single thimble gives a dominant contribution to the path integral and we identify it, we can numerically evaluate the path integral.

As one of the approach to evaluate the path integral, we consider the hybrid Monte Carlo algorithm on the Lefschetz thimble, in which configurations are proposed with the high acceptance rate. Since we need to compute the inverse of tangent vectors and the Jacobian determinant using the LU decomposition, its computational cost is $\mathcal{O}(n^3)$. If many thimbles contribute to the path integral, however, the original idea of the Lefschetz thimble method does not work well. Also the identification of the thimble which gives a dominant contribution is a hard task, in general.

In Chapter 3, we consider the generalized Lefschetz thimble method, where the contribution of multiple thimbles are included in the path integral and the identification of

the thimble is not necessary. The point of this improved method is to find a integration contour which is a connected region, and on which the fluctuation of the phase is mild. To find such a contour we consider a point on the original integration contour as an initial condition of the gradient flow. Then flowing each point on the original integration contour, we obtain a deformed contour. The deformed contour approaches the Lefschetz thimbles contributing to the path integral, and by adjusting the flow time we observe that it is a connected region. Since a point on the original integration contour is mapped to a point on the deformed contour by a diffeomorphism, we can change the complex integration variables on the curved space back to the real variables. Thus by using the real variables we do not need to solve the equation of the motion for the constraint system. We consider the Metropolis method with the real variables, where the update requires $\mathcal{O}(n^2)$ computation. The distribution of the proposed configuration on the flowed contour is anisotropic for a large flow time, and the sampling is inefficient. However, as opposed to the simulation on the curved space, this method has the advantage that for the arbitrary random numbers we always find a proposed configuration on the flowed contour, as long as the original integration contour and the flowed contour have a one-to-one correspondence.

In Chapter 4, we discuss the gradient flow without the blow-up. In the generalized Lefschetz thimble method, we use the gradient flow to deform the contour. However, as the flow time increase, the flowed contour approaches infinity or zeros of the fermion determinant, and divided by them in a finite flow time. Thus the sequence of the configuration is trapped to the restricted region, and the situation is the same as in the original Lefschetz thimble method. The divergence of the action in a finite flow time is called the blow-up. To prevent the blow-up, we introduce an alternative flow equation. The point of this flow is a flow factor in the force term, which is a function with respect to the complexified variables, and suppressed in the vicinity of infinity and zeros of the fermion determinant.

In Chapter 5, we construct an algorithm which evaluate the path integral using the gradient flow without the blow-up. Based on the hybrid Monte Carlo algorithm on the Lefschetz thimble, we construct the hybrid Monte Carlo algorithm on the flowed contour without the blow-up. The algorithm we construct is different from the conventional one in that the reality condition is not satisfied for the gradient flow without the blow-up. Thus to project a momentum on the tangent space, we compute the QR decomposition of the tangent vectors, whereas in the conventional gradient flow we compute the inverse of the tangent vectors. In order to confirm the validity of the algorithm we construct, we first apply it to the Thirring model in the uniformed subspace, where the path integral is given on the one-dimensional space, and then to the Thirring model, where the path integral is given on the multi-dimensional space. We show that the result we obtain agree with the analytic result, as opposed to the conventional generalized Lefschetz thimble method. Therefore it shows that the contributions of the multiple thimbles are correctly included in the numerical evaluation.

However the algorithm we construct has some week points. Firstly, the computational cost is potentially expensive. In the computation of the gradient flow equation we adopt, we need to compute the fermion determinant iteratively. Secondly, the contour may be strongly curved depending on the regularization parameters in the flow equation and the flow time. For the strongly curved contour, we take a sufficiently small step size to solve the molecular dynamics, or we cannot project the momentum on the contour. We need to overcome these week points, and leave them for a future study.

We also need to confirm that the algorithm is applicable to a wide range of models. For a future study, it would be interesting to apply the hybrid Monte Carlo algorithm without the blow-up to the other models such as the chiral random matrix model [55, 56], which is a toy model of finite-density QCD. We believe that the algorithm using the gradient flow without the blow-up is promising approach to solve the sign problem and by developing and improving it we can apply it to finite-density QCD in future.

Appendix A

Metropolis algorithm on generalized surface

In the Metropolis method, we accept a proposed configuration x_B, which is generated from the configuration x_A by a probability,

$$P_{\rm acc}(x_A \to x_B) = \min\left\{1, e^{-S(x_B)}/e^{-S(x_A)}\right\}. \tag{A.1}$$

Here we denote the transition probability from x_A to x_B as $T(x_A \to x_B)$. Then we note that in order to satisfy the detailed balanced condition,

$$e^{-S(x_A)}T(x_A \to x_B) = e^{-S(x_B)}T(x_B \to x_A), \tag{A.2}$$

the probability $P(x_A \to x_B)$ of generating a configuration x_B from a configuration x_A need to be equivalent to the probability $P(x_B \to x_A)$ of generating a configuration x_A from a configuration x_B. If we have $P(x_A \to x_B) \neq P(x_B \to x_A)$, after generating the configuration x_B from the configuration x_A we accept it by a probability,

$$P_{\rm corr}(x_A \to x_B) = \min\left\{1, P(x_B \to x_A)/P(x_A \to x_B)\right\}. \tag{A.3}$$

Thus we need to accept the proposal twice to update the configuration, and the transition probability from x_A to x_B is written as

$$T(x_A \to x_B) = P(x_A \to x_B)P_{\rm corr}(x_A \to x_B)P_{\rm acc}(x_A \to x_B), \tag{A.4}$$

and the detailed balanced condition is satisfied. On the curved space, the method of proposing a new configuration is important. Here we consider the method in which we can adopt the proposal used in the hybrid Monte Carlo algorithm on the curved space in Sec. 5.1.

First, we generate a complex momentum w on the tangent space $T_z\Sigma$. One may consider to generate it by the Gaussian distribution, but the momentum can be arbitrarily

large. For a large momentum, possibly we may not find a proposal. Thus here we generate a complex momentum by a uniform distribution with a small radius r as [1)]

$$P_{\rm unif}(w) = \begin{cases} \text{const.} & (\|w\| \le r), \\ 0 & (\|w\| > r). \end{cases} \tag{A.5}$$

The generated momentum w is projected on the tangent space $T_z\Sigma$ using the projector (5.12). To propose a configuration, we update the pair (z, w) by the equations,

$$w_i(n+1/2) = w_i(n) - 1/2\Delta\tau\tilde{Q}_i^\alpha(z(n))\lambda_1^\alpha, \tag{A.6}$$
$$z_i(n+1) = z_i(n) + \Delta\tau w_i(n+1/2), \tag{A.7}$$
$$w_i(n+1) = w_i(n+1/2) - 1/2\Delta\tau\tilde{Q}_i^\alpha(z(n+1))\lambda_2^\alpha. \tag{A.8}$$

The equations are same as the equations of motion of molecular dynamics (5.17)-(5.19) without the force term $(\partial S(z(n))/\partial z)^*$, and we can solve them using the iterative method such as the fixed point iteration method and the Newton's method.

If the solution is unique, Eqs. (A.6)-(A.8) are reversible. Then using the reversibility and accepting the proposal by the probability,

$$P_{\rm corr}(\Phi_A \to \Phi_B) = \min\left\{1, P_{\rm unif}(w_B)/P_{\rm unif}(w_A)\right\}, \tag{A.9}$$

the detailed balance condition (A.2) is satisfied. Here we write $\Phi = (z, w)$ for simplicity. The transition probability from x_A to x_B is written as

$$\begin{aligned} &T(x_A \to x_B) \\ &= P_{\rm acc}(z_A \to z_B) \int dw_A dw_B\, P_{\rm unif}(w_A) P_M(\Phi_A \to \Phi_B) P_{\rm corr}(\Phi_A \to \Phi_B), \end{aligned} \tag{A.10}$$

where P_M is the probability to choose the configuration (z_B, w_B),

$$P_M(\Phi_A \to \Phi_B) = \delta^{(2n)}(\Phi_A - F(\Phi_B)). \tag{A.11}$$

F denotes the map given by Eqs. (A.6)-(A.8). Here we decompose the momentum as $w_i = Q_i^\alpha p^\alpha$, and define the measure by $dw = d^n p$. Then we prove that the detailed

[1)] For example, by generating n unit Gaussian random numbers p_i $(i = 1, \ldots, n)$ and a uniform random number r in the interval $[0, 1]$, we have the complex vector $w_i = Q_i^\alpha p^\alpha$ using the orthonormal basis $\{Q_i^\alpha\}$ given by the QR decomposition (5.8). Then, we normalize the momenta as $w_i \to r^{1/n}(w_i/\|w\|)$.

balance condition is satisfied as follows:

$$
\begin{aligned}
& e^{-S(x_A)} T(x_A \to x_B) \\
&= e^{-S(x_A)} P_{\text{acc}}(z_A \to z_B) \int dw_A dw_B \, P_{\text{unif}}(w_A) P_M(\Phi_A \to \Phi_B) P_{\text{corr}}(\Phi_A \to \Phi_B) \qquad \text{(A.12)} \\
&= e^{-S(x_B)} P_{\text{acc}}(z_B \to z_A) \int dw_A dw_B \, P_{\text{unif}}(w_A) P_M(\Phi_A \to \Phi_B) P_{\text{corr}}(\Phi_A \to \Phi_B) \qquad \text{(A.13)} \\
&= e^{-S(x_B)} P_{\text{acc}}(z_B \to z_A) \int dw_A dw_B \, P_{\text{unif}}(w_A) P_M(\Phi_B \to \Phi_A) P_{\text{corr}}(\Phi_A \to \Phi_B) \qquad \text{(A.14)} \\
&= e^{-S(x_B)} P_{\text{acc}}(z_B \to z_A) \int dw_A dw_B \, P_{\text{unif}}(w_B) P_M(\Phi_B \to \Phi_A) P_{\text{corr}}(\Phi_B \to \Phi_A). \qquad \text{(A.15)}
\end{aligned}
$$

To derive the relation above we used $P_M((z_A, w_A) \to (z_B, w_B)) = P_M((z_B, -w_B) \to (z_A, -w_A))$, and $P_{\text{unif}}(-w) = P_{\text{unif}}(w)$.

Bibliography

[1] J. R. Klauder, *Stochastic Quantization*, *Acta Phys. Austriaca Suppl.* **25** (1983) 251–281.

[2] G. Parisi, *On complex probabilities*, *Phys. Lett. B* **131** (1983) 393–395.

[3] G. Parisi and Y.-s. Wu, *Perturbation Theory Without Gauge Fixing*, *Sci. Sin.* **24** (1981) 483.

[4] G. Aarts, E. Seiler and I.-O. Stamatescu, *The Complex Langevin method: When can it be trusted?*, *Phys. Rev. D* **81** (2010) 054508, [0912.3360].

[5] G. Aarts, F. A. James, E. Seiler and I.-O. Stamatescu, *Complex Langevin: Etiology and Diagnostics of its Main Problem*, *Eur. Phys. J. C* **71** (2011) 1756, [1101.3270].

[6] K. Nagata, J. Nishimura and S. Shimasaki, *Argument for justification of the complex Langevin method and the condition for correct convergence*, *Phys. Rev. D* **94** (2016) 114515, [1606.07627].

[7] C. E. Berger, L. Rammelmüller, A. C. Loheac, F. Ehmann, J. Braun and J. E. Drut, *Complex Langevin and other approaches to the sign problem in quantum many-body physics*, 1907.10183.

[8] AuroraScience collaboration, M. Cristoforetti, F. Di Renzo and L. Scorzato, *New approach to the sign problem in quantum field theories: High density QCD on a Lefschetz thimble*, *Phys. Rev. D* **86** (2012) 074506, [1205.3996].

[9] M. Cristoforetti, F. Di Renzo, A. Mukherjee and L. Scorzato, *Monte Carlo simulations on the Lefschetz thimble: Taming the sign problem*, *Phys. Rev. D* **88** (2013) 051501, [1303.7204].

[10] A. Alexandru, G. Basar and P. Bedaque, *Monte Carlo algorithm for simulating fermions on Lefschetz thimbles*, *Phys. Rev. D* **93** (2016) 014504, [1510.03258].

[11] H. Fujii, D. Honda, M. Kato, Y. Kikukawa, S. Komatsu and T. Sano, *Hybrid Monte Carlo on Lefschetz thimbles - A study of the residual sign problem*, *JHEP* **10** (2013) 147, [1309.4371].

[12] A. Alexandru, G. Basar, P. F. Bedaque, G. W. Ridgway and N. C. Warrington, *Sign problem and Monte Carlo calculations beyond Lefschetz thimbles*, *JHEP* **05** (2016) 053, [1512.08764].

[13] A. Alexandru, G. Basar, P. F. Bedaque and N. C. Warrington, *Tempered transitions between thimbles*, *Phys. Rev. D* **96** (2017) 034513, [1703.02414].

[14] M. Fukuma and N. Umeda, *Parallel tempering algorithm for integration over Lefschetz thimbles*, *PTEP* **2017** (2017) 073B01, [1703.00861].

[15] M. Fukuma, N. Matsumoto and N. Umeda, *Implementation of the HMC algorithm on the tempered Lefschetz thimble method*, 1912.13303.

[16] M. Fukuma and N. Matsumoto, *Worldvolume approach to the tempered Lefschetz thimble method*, 2012.08468.

[17] A. Alexandru, P. F. Bedaque, H. Lamm and S. Lawrence, *Deep Learning Beyond Lefschetz Thimbles*, *Phys. Rev. D* **96** (2017) 094505, [1709.01971].

[18] A. Alexandru, P. F. Bedaque, H. Lamm and S. Lawrence, *Finite-Density Monte Carlo Calculations on Sign-Optimized Manifolds*, *Phys. Rev. D* **97** (2018) 094510, [1804.00697].

[19] A. Alexandru, P. F. Bedaque, H. Lamm, S. Lawrence and N. C. Warrington, *Fermions at Finite Density in 2+1 Dimensions with Sign-Optimized Manifolds*, *Phys. Rev. Lett.* **121** (2018) 191602, [1808.09799].

[20] Y. Mori, K. Kashiwa and A. Ohnishi, *Toward solving the sign problem with path optimization method*, *Phys. Rev. D* **96** (2017) 111501, [1705.05605].

[21] Y. Mori, K. Kashiwa and A. Ohnishi, *Application of a neural network to the sign problem via the path optimization method*, *PTEP* **2018** (2018) 023B04, [1709.03208].

[22] K. Kashiwa, Y. Mori and A. Ohnishi, *Controlling the model sign problem via the path optimization method: Monte Carlo approach to a QCD effective model with Polyakov loop*, *Phys. Rev. D* **99** (2019) 014033, [1805.08940].

[23] K. Kashiwa, Y. Mori and A. Ohnishi, *Application of the path optimization method to the sign problem in an effective model of QCD with a repulsive vector-type interaction*, *Phys. Rev. D* **99** (2019) 114005, [1903.03679].

[24] Y. Mori, K. Kashiwa and A. Ohnishi, *Path optimization in $0+1D$ QCD at finite density*, *PTEP* **2019** (2019) 113B01, [1904.11140].

[25] A. Alexandru, G. Basar, P. F. Bedaque and N. C. Warrington, *Complex Paths Around The Sign Problem*, 2007.05436.

[26] Y. Tanizaki, H. Nishimura and J. J. Verbaarschot, *Gradient flows without blow-up for Lefschetz thimbles*, *JHEP* **10** (2017) 100, [1706.03822].

[27] R. P. Feynman, *Space-time approach to nonrelativistic quantum mechanics*, *Rev. Mod. Phys.* **20** (1948) 367–387.

[28] R. P. Feyn mann and A. R. Hibbs, *Quantum Mechanics and Path Integrals*. McGraw-Hill, 1965.

[29] J. S. Schwinger, *Brownian motion of a quantum oscillator*, *J. Math. Phys.* **2** (1961) 407–432.

[30] L. Keldysh, *Diagram technique for nonequilibrium processes*, *Zh. Eksp. Teor. Fiz.* **47** (1964) 1515–1527.

[31] J. Berges and I.-O. Stamatescu, *Simulating nonequilibrium quantum fields with stochastic quantization techniques*, *Phys. Rev. Lett.* **95** (2005) 202003, [hep-lat/0508030].

[32] J. Berges, S. Borsanyi, D. Sexty and I.-O. Stamatescu, *Lattice simulations of real-time quantum fields*, *Phys. Rev. D* **75** (2007) 045007, [hep-lat/0609058].

[33] Z.-G. Mou, P. M. Saffin, A. Tranberg and S. Woodward, *Real-time quantum dynamics, path integrals and the method of thimbles*, *JHEP* **06** (2019) 094, [1902.09147].

[34] A. Alexandru, G. Basar, P. F. Bedaque, S. Vartak and N. C. Warrington, *Monte Carlo Study of Real Time Dynamics on the Lattice*, *Phys. Rev. Lett.* **117** (2016) 081602, [1605.08040].

[35] A. Alexandru, G. Basar, P. F. Bedaque and G. W. Ridgway, *Schwinger-Keldysh formalism on the lattice: A faster algorithm and its application to field theory*, *Phys. Rev. D* **95** (2017) 114501, [1704.06404].

[36] F. Pham, *Vanishing Homologies And The n Variable Saddlepoint Method*, *Proc. Symp. Pure Math.* **40** (1983) 319–333.

[37] E. Witten, *Analytic Continuation Of Chern-Simons Theory*, *AMS/IP Stud. Adv. Math.* **50** (2011) 347–446, [1001.2933].

[38] T. Takagi, *On an Algebraic Problem Reluted to an Analytic Theorem of Carathéodory and Fejér and on an Allied Theorem of Landau*, *Japanese journal of mathematics: transactions and abstracts* **1** (1924) 83–93.

[39] S. Duane, A. Kennedy, B. Pendleton and D. Roweth, *Hybrid Monte Carlo*, *Phys. Lett. B* **195** (1987) 216–222.

[40] H. Fujii, S. Kamata and Y. Kikukawa, *Lefschetz thimble structure in one-dimensional lattice Thirring model at finite density*, *JHEP* **11** (2015) 078, [1509.08176].

[41] H. Fujii, S. Kamata and Y. Kikukawa, *Monte Carlo study of Lefschetz thimble structure in one-dimensional Thirring model at finite density*, *JHEP* **12** (2015) 125, [1509.09141].

[42] M. Grady, *A Fast Algorithm for Monte Carlo Simulations of Systems With Fermions*, *Phys. Rev. D* **32** (1985) 1496.

[43] M. Cristoforetti, F. Di Renzo, G. Eruzzi, A. Mukherjee, C. Schmidt, L. Scorzato et al., *An efficient method to compute the residual phase on a Lefschetz thimble*, *Phys. Rev. D* **89** (2014) 114505, [1403.5637].

[44] W. E. Thirring, *A Soluble relativistic field theory?*, *Annals Phys.* **3** (1958) 91–112.

[45] J. M. Pawlowski and C. Zielinski, *Thirring model at finite density in 0+1 dimensions with stochastic quantization: Crosscheck with an exact solution*, *Phys. Rev. D* **87** (2013) 094503, [1302.1622].

[46] J. M. Pawlowski and C. Zielinski, *Thirring model at finite density in 2+1 dimensions with stochastic quantization*, *Phys. Rev. D* **87** (2013) 094509, [1302.2249].

[47] J. M. Pawlowski, I.-O. Stamatescu and C. Zielinski, *Simple QED- and QCD-like Models at Finite Density*, *Phys. Rev. D* **92** (2015) 014508, [1402.6042].

[48] A. Alexandru, G. Basar, P. F. Bedaque, G. W. Ridgway and N. C. Warrington, *Monte Carlo calculations of the finite density Thirring model*, *Phys. Rev. D* **95** (2017) 014502, [1609.01730].

[49] P. Hasenfratz and F. Karsch, *Chemical Potential on the Lattice*, *Phys. Lett. B* **125** (1983) 308–310.

[50] K. G. Wilson, *Quarks and strings on a lattice*, in *New phenomena in subnuclear physics*, pp. 69–142. Springer, 1977.

[51] J. B. Kogut and L. Susskind, *Hamiltonian Formulation of Wilson's Lattice Gauge Theories*, *Phys. Rev. D* **11** (1975) 395–408.

[52] L. Susskind, *Lattice Fermions*, *Phys. Rev.* **D16** (1977) 3031–3039.

[53] H. B. Nielsen and M. Ninomiya, *Absence of Neutrinos on a Lattice. 1. Proof by Homotopy Theory*, *Nucl. Phys.* **B185** (1981) 20.

[54] H. B. Nielsen and M. Ninomiya, *Absence of Neutrinos on a Lattice. 2. Intuitive Topological Proof*, *Nucl. Phys.* **B193** (1981) 173–194.

[55] M. A. Stephanov, *Random matrix model of QCD at finite density and the nature of the quenched limit*, *Phys. Rev. Lett.* **76** (1996) 4472–4475, [hep-lat/9604003].

[56] A. M. Halasz, A. Jackson, R. Shrock, M. A. Stephanov and J. Verbaarschot, *On the phase diagram of QCD*, *Phys. Rev. D* **58** (1998) 096007, [hep-ph/9804290].